AD-A057 249 MASSACHUSETTS UNIV AMHERST ASTRONOMY RESEARCH FACILITY F/G 4/1
THEORETICAL STUDY OF BACKGROUND RADIANCE IN UPPER ATMOSPHERE.(U)
DEC 77 P HANSEN, R LAUZZANA, H SAKAI F19628-75-C-0187
UNCLASSIFIED UMASS-ARF-77-304 AFGL-TR-78-0013 NL

1 OF 1
AD
A057 249

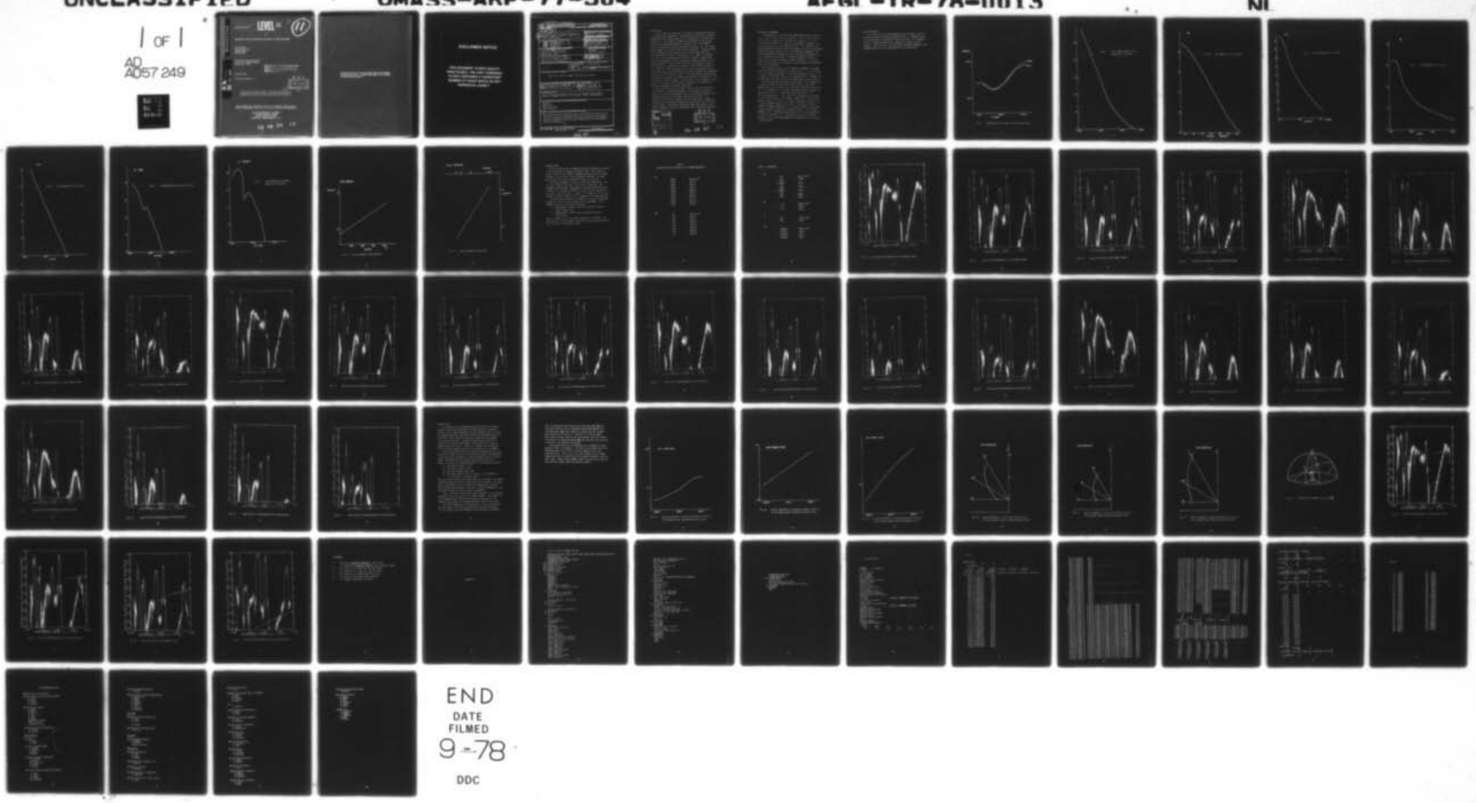

END
DATE
FILMED
9-78
DDC

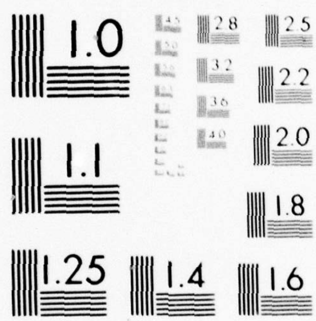
1.0
1.1
1.25
1.4
1.6
1.8
2.0
2.2
2.5
2.8
3.2
3.6
4.0

AD A057249

AD No.
DDC FILE COPY

AFGL-TR-78-0013

LEVEL II

(11)

THEORETICAL STUDY OF BACKGROUND RADIANCE IN UPPER ATMOSPHERE

Peter Hansen
Raymond Lauzzana
Hajime Sakai
John Strong

Astronomy Research Facility
University of Massachusetts
Amherst MA 01003



December 1977

Scientific Report No. 1



Approved for public release; distribution unlimited.

This research was sponsored in part by the Defense Nuclear Agency
Subtask I25AAXHX632, Work Unit 42, entitled "SPIRE Instrumentation."

AIR FORCE GEOPHYSICS LABORATORY
AIR FORCE SYSTEMS COMMAND
UNITED STATES AIR FORCE
HANSCOM AFB, MASSACHUSETTS 01731

78 08 03 19

# DISCLAIMER NOTICE

UNCLASSIFIED

SECURITY CLASSIFICATION OF THIS PAGE (When Data Entered)

## REPORT DOCUMENTATION PAGE

READ INSTRUCTIONS BEFORE COMPLETING FORM

18 19

**1. REPORT NUMBER:** AFGL-TR-78-0013

**2. GOVT ACCESSION NO.:**

**3. RECIPIENT'S CATALOG NUMBER:**

**4. TITLE (and Subtitle):** 6 THEORETICAL STUDY OF BACKGROUND RADIANCE IN UPPER ATMOSPHERE

**5. TYPE OF REPORT & PERIOD COVERED:** 9 Interim Scientific Report, No. 1

**6. PERFORMING ORG. REPORT NUMBER:** 14 UMASS-ARF-77-304

**7. AUTHOR(s):** 10 Peter Hansen, Raymond Lauzzana, Hajime Sakai, John Strong

**8. CONTRACT OR GRANT NUMBER(s):** 15 F19628-75-C-0187

**9. PERFORMING ORGANIZATION NAME AND ADDRESS:**
Astronomy Research Facility
University of Massachusetts
Amherst MA 01003

**10. PROGRAM ELEMENT, PROJECT, TASK AREA & WORK UNIT NUMBERS:**
PE61102F
2310G404 & 2310G408

**11. CONTROLLING OFFICE NAME AND ADDRESS:**
Air Force Geophysics Laboratory
Hanscom AFB, Massachusetts 01731
Monitor/Richard Nadile/OPR-1

**12. REPORT DATE:** 11 Dec[redacted]77

**13. NUMBER OF PAGES:** 69

**14. MONITORING AGENCY NAME & ADDRESS (if different from Controlling Office):**
12 67p.
61102F

**15. SECURITY CLASS. (of this report):** Unclassified

**15a. DECLASSIFICATION/DOWNGRADING SCHEDULE:**

**16. DISTRIBUTION STATEMENT (of this Report):**

Approved for public release; distribution unlimited.

**17. DISTRIBUTION STATEMENT (of the abstract entered in Block 20, if different from Report):**
16 2310, I25AAXH 17 G4, X632

**18. SUPPLEMENTARY NOTES:**
This research was sponsored in part by the Defense Nuclear Agency Subtask I25AAXHX632, Work Unit 42, entitled "SPIRE Instrumentation."

**19. KEY WORDS (Continue on reverse side if necessary and identify by block number):**
Infrared
Scattering
Emission spectra
Upper atmosphere

**20. ABSTRACT (Continue on reverse side if necessary and identify by block number):**

The Infrared Background Radiance level in the atmosphere above 60 km is estimated for various sight conditions using the two existing computer codes, the FLASH and the DEGGES. The actual computations were made by using the programs modified from these original codes for improvement of processing efficiency.

DD FORM 1473, 1 JAN 73 EDITION OF 1 NOV 65 IS OBSOLETE
S/N 0102-014-6601

UNCLASSIFIED

SECURITY CLASSIFICATION OF THIS PAGE (When Data Entered)

406 989

INTRODUCTION

Two processes are responsible for causing the background radiation of the upper earth atmosphere: the atmospheric scattering of the solar radiation and the natural emission by the atmospheric constituent gas molecules.[1,2] Two computer programs were developed for theoretical study of the atmospheric background radiance level. The FLASH,[3-6] which was developed by Radiation Research Associates, Inc., Fort Worth, Texas, computes the level of the scattered radiation. Its applicability has not been extensively tested in the infrared region where the scattered radiation level is significantly low. Degges of Visidyne, Inc., Burlington, Massachusetts, developed a computer program which produces an estimated level of the molecular emission radiance in the upper atmosphere.[7] The solution produced by the DEGGES (we refer to his program as the DEGGES in this report) covers a spectral region of $400 \sim 4000\ cm^{-1}$. The scattering process plays a predominant role in higher $cm^{-1}$ range, while the molecular emission dominates the background radiance level in lower $cm^{-1}$ region. Contribution from both processes is expected to equalize in a range between $3000\ cm^{-1}$ and $5000\ cm^{-1}$. The present work intends to make a critical study of both programs in this region. It is hoped that the results obtained by both programs are eventually combined in a proper perspective.

This report describes the results which we obtained during the first stage of our multiyear program. Our main effort during this stage was to modify both programs into a form readily adaptable to our computing facility, the CDC 6600 operated under the NOS 1 2, in addition to familiarize ourselves with their algorithms. Several IO operations in the original programs were found rather inefficient and time-consuming. Significant improvements have been achieved in the overall computation speed by streamlining these inefficient operations.

ATMOSPHERIC PARAMETERS

The basic physics involved in the scattering and the molecular emission process are well known in general. Both programs, FLASH and DEGGES, need a parametrized knowledge of the atmosphere in which these processes take place. Some of the atmospheric parameters are, at present, known only in a limited accuracy. It is desirable that both programs perform their computations based on a unified atmospheric model by using an identical set of the atmospheric parameters, and rather unfortunate at present that there exist some discrepancies in these parameters used by them. The SPIRE program was planned to provide us an improved knowledge of these parameters. It is hoped that the data analysis to be conducted in this study would eventually bring their improvement.

The temperature profile of the atmosphere assumed in the FLASH and in the DEGGES are different, as shown in Fig. 1. The profile may be of a secondary significance in the FLASH computation, while it is to produce a first-order effect on the computation by the DEGGES. No attempts have been made to run both programs using a unified profile.

The total gas density present in each layer of the atmosphere is an important parameter which affects the accuracy of the FLASH computation, while the data on the individual constituent species are not for the computation of the upper atmosphere scattering where the molecular absorption is a negligibly small correction to the scattering computation. Fig. 2 shows the total gas density assumed in the FLASH calculation. The chemical composition of each species given as a function of the altitude must be precisely known in order to make the DEGGES computation realistic. The total gas density affects the DEGGES computation if a significant amount of the energy transfers between the molecules through collisions. In the upper atmosphere the collisional processes affect little to the problem of the radiative balance. Fig. 3 through Fig. 8 show the molecular density of various species assumed by the DEGGES given as a function of the altitude.

SOLAR IRRADIANCE

The solar radiation is the primary and the secondary source for the upper atmosphere background radiation which is originated either by the scattering or the molecular emission process. The irradiance value is a parameter affecting the computation accuracy of both programs. Fig. 9 and Fig. 10 show the solar irradiance assumed in both programs given as a unit or $watt/cm^2/cm^{-1}$ and of $watt/cm^2/\mu$.

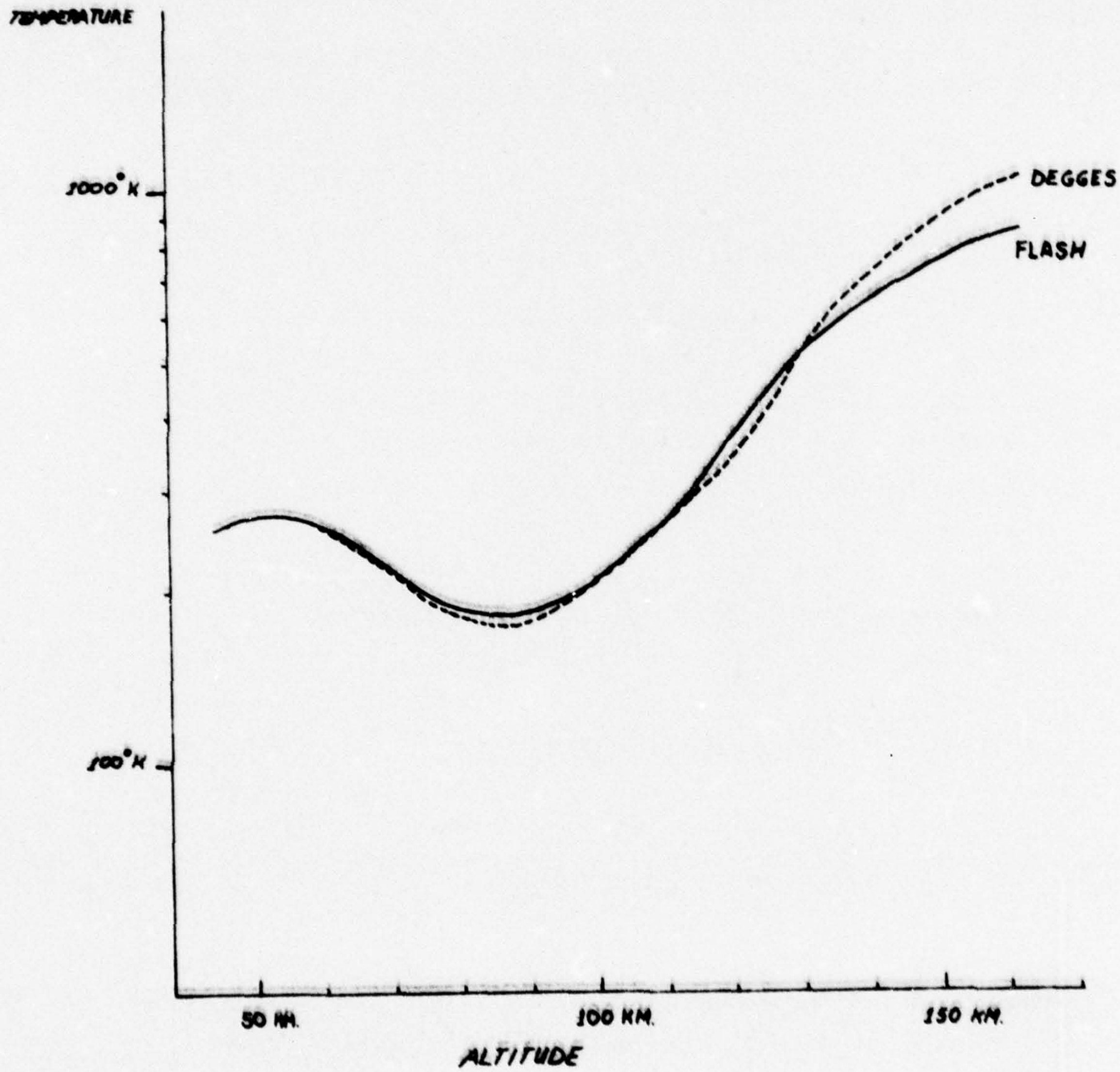


Fig. 1 Temperature Profile used in the two computations

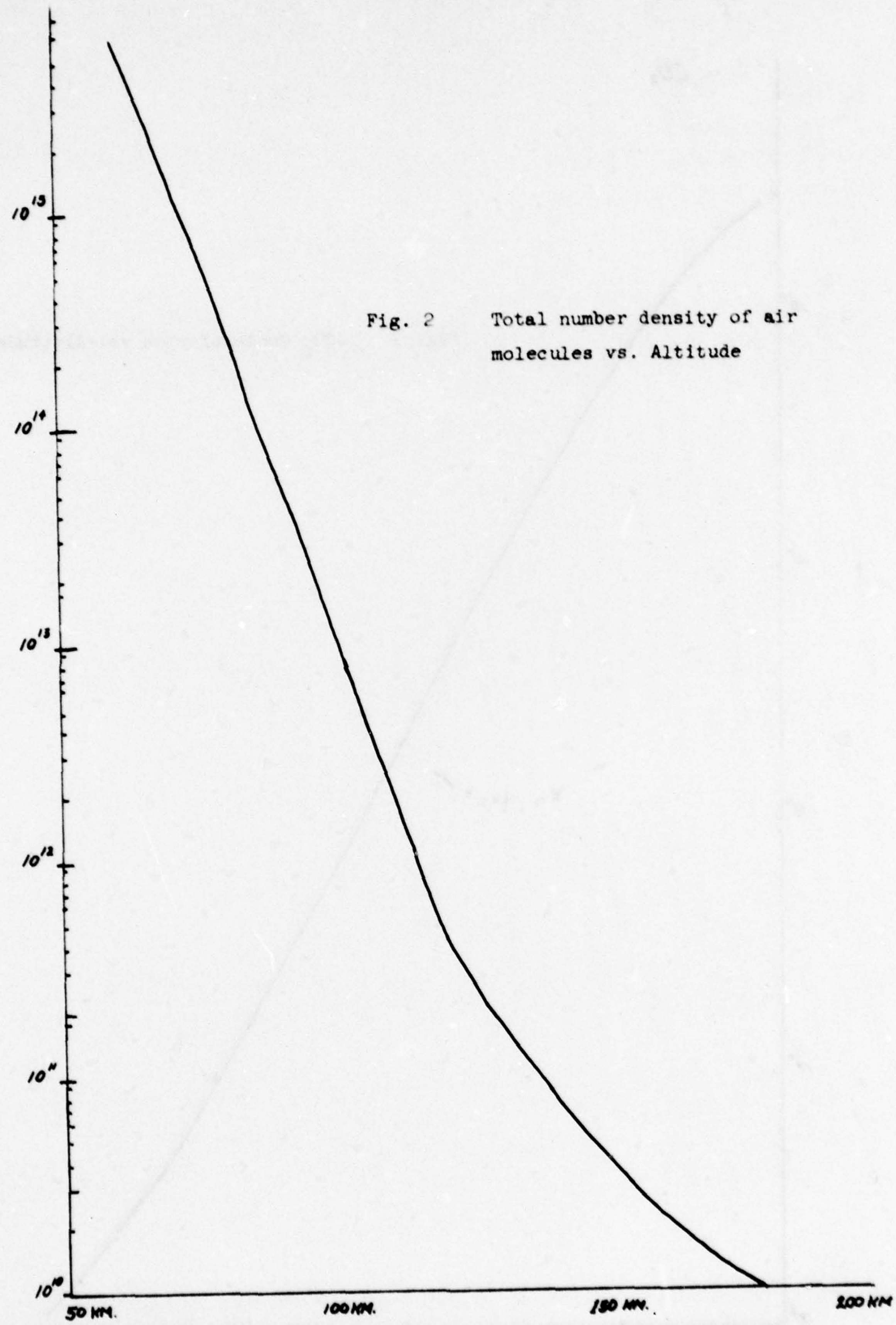


Fig. 2 Total number density of air molecules vs. Altitude

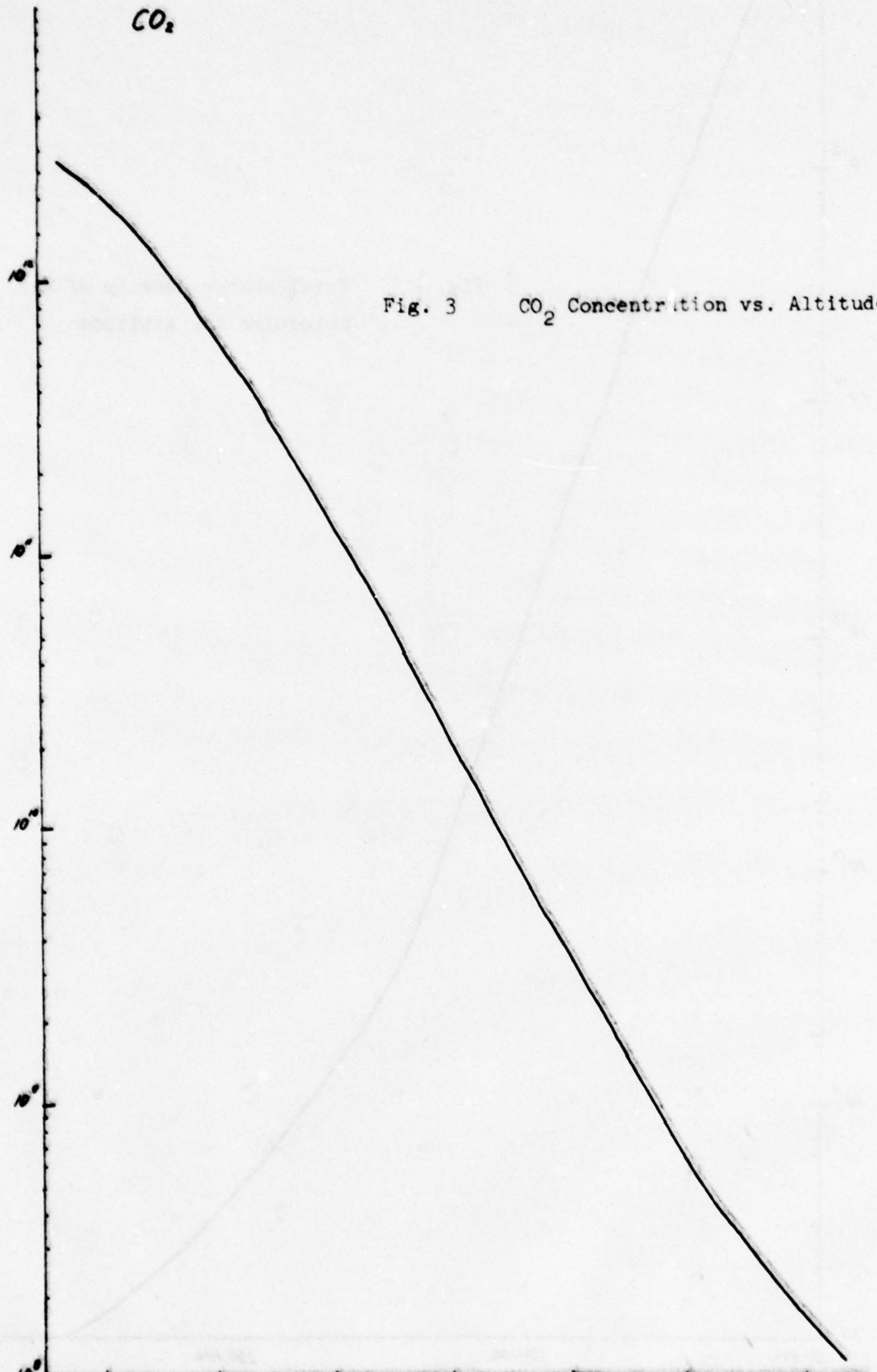


Fig. 3 $CO_2$ Concentration vs. Altitude

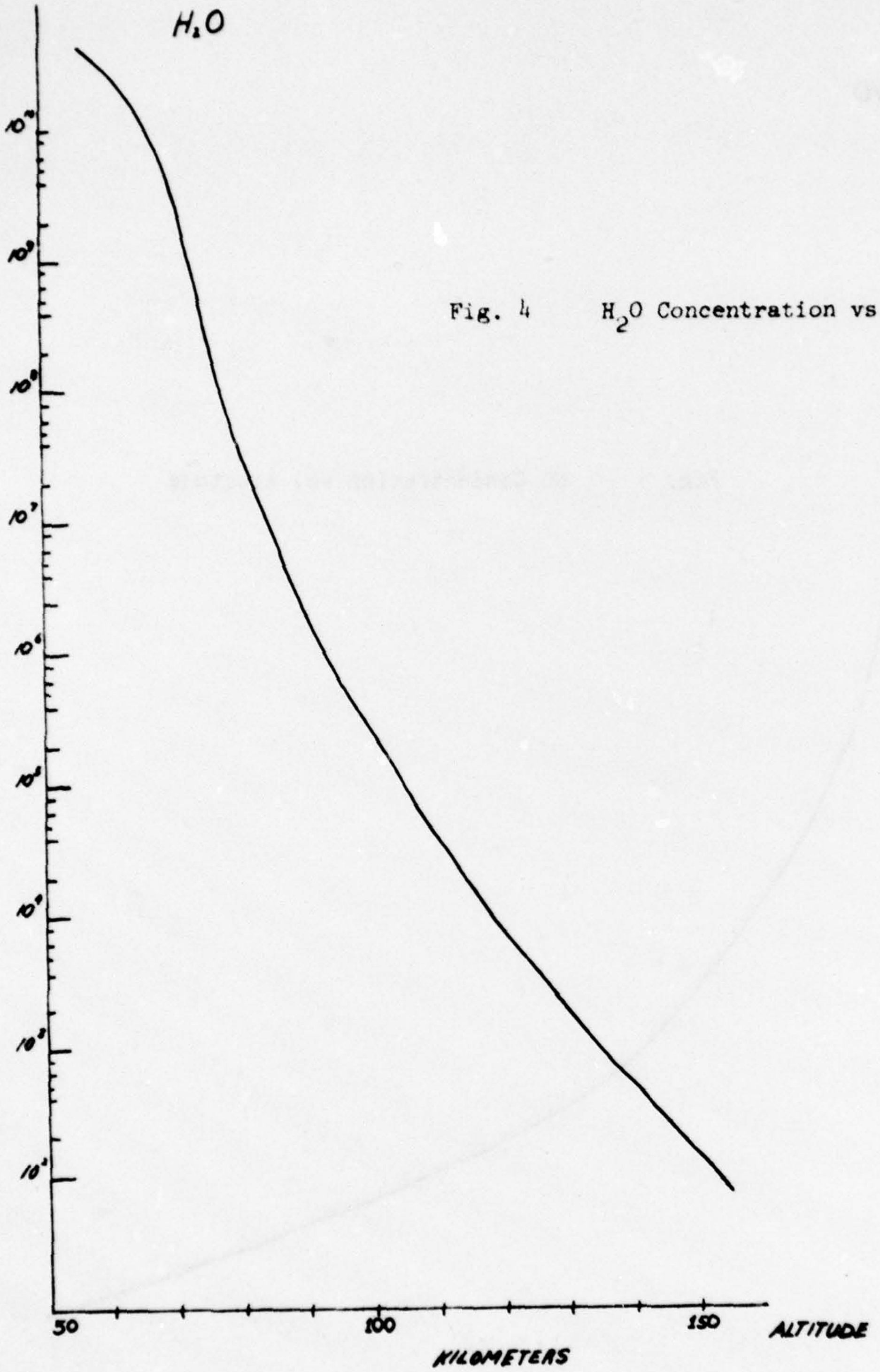


Fig. 4 $H_2O$ Concentration vs. Altitude

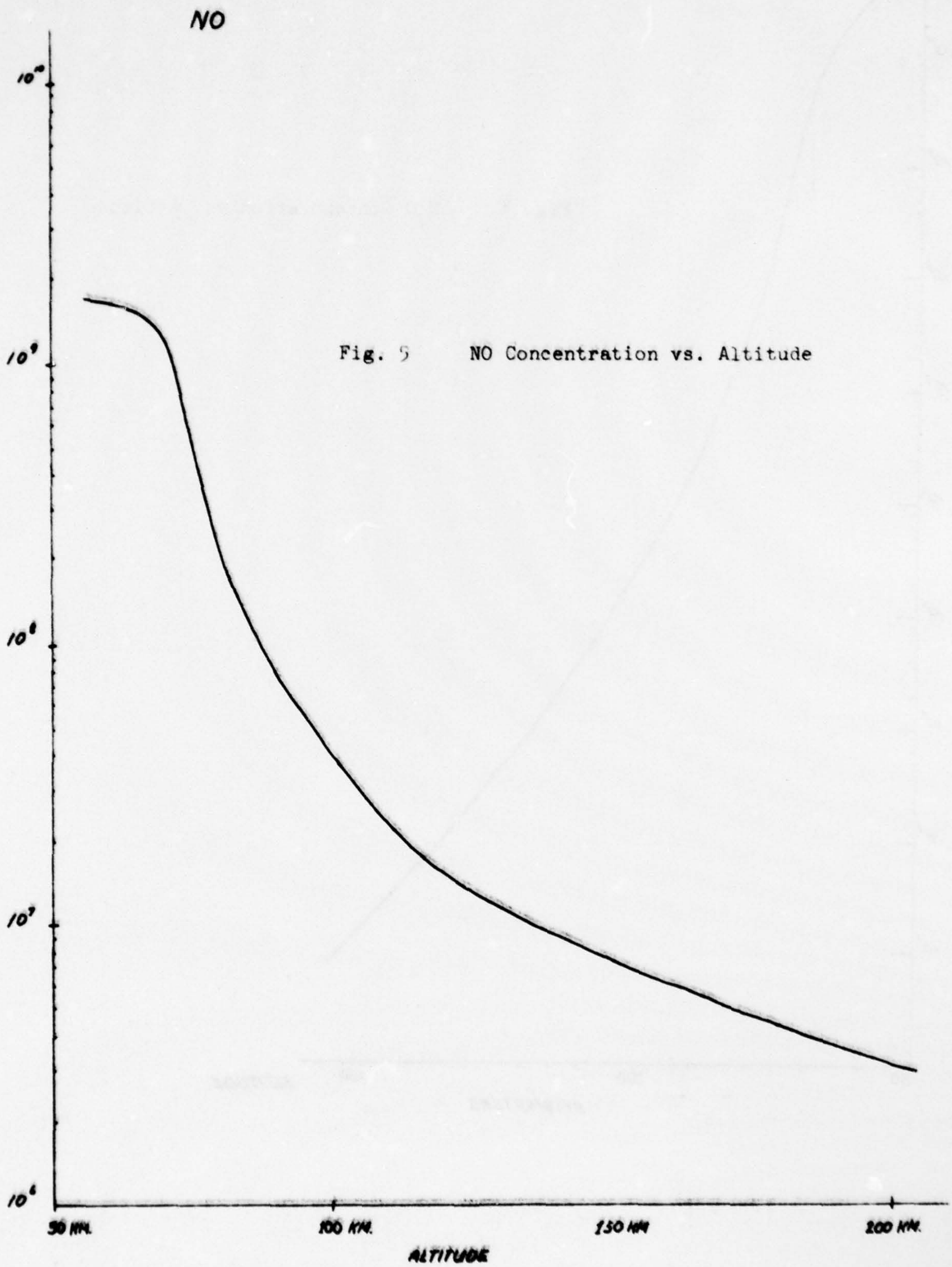


Fig. 5 NO Concentration vs. Altitude

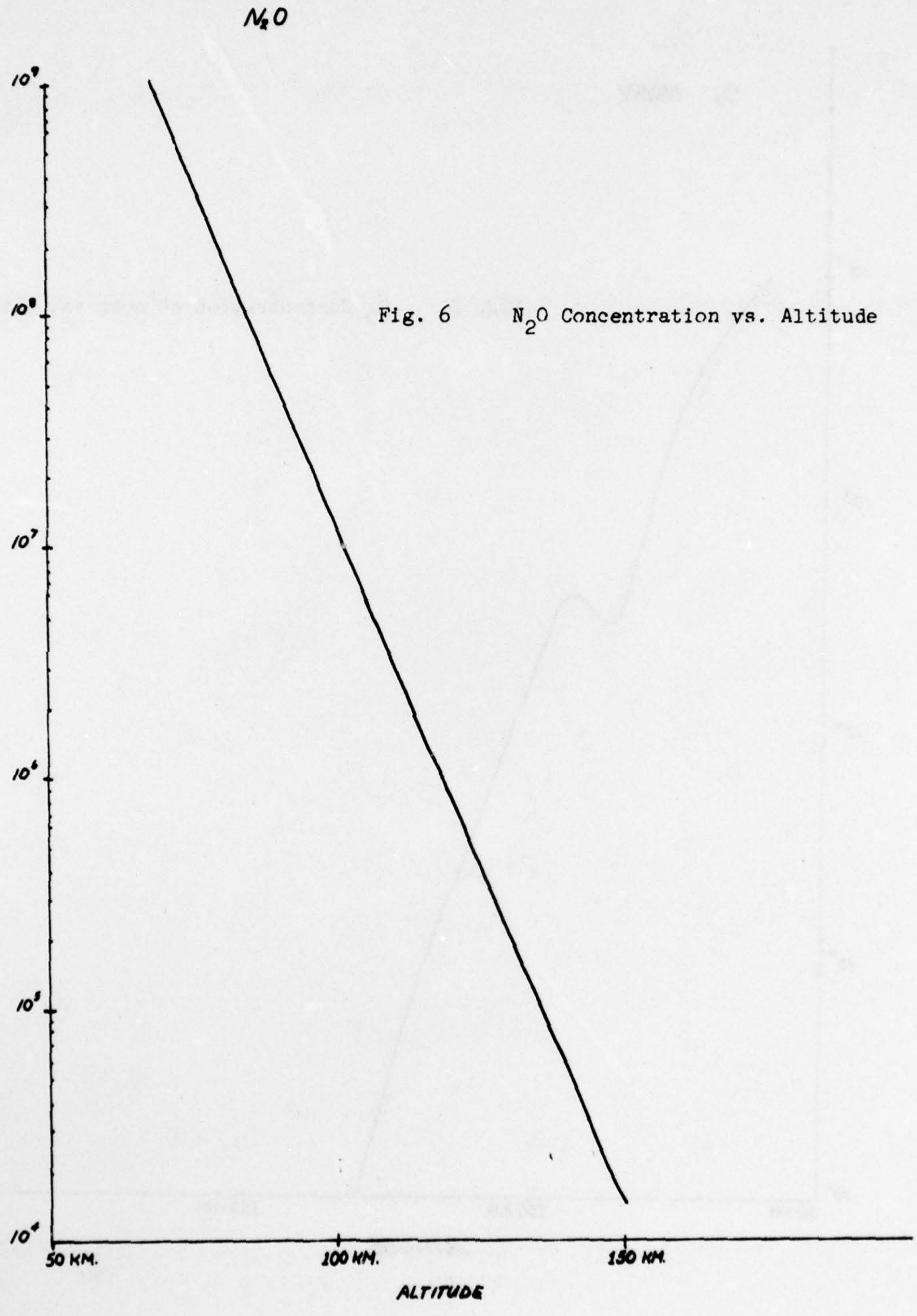


Fig. 6 $N_2O$ Concentration vs. Altitude

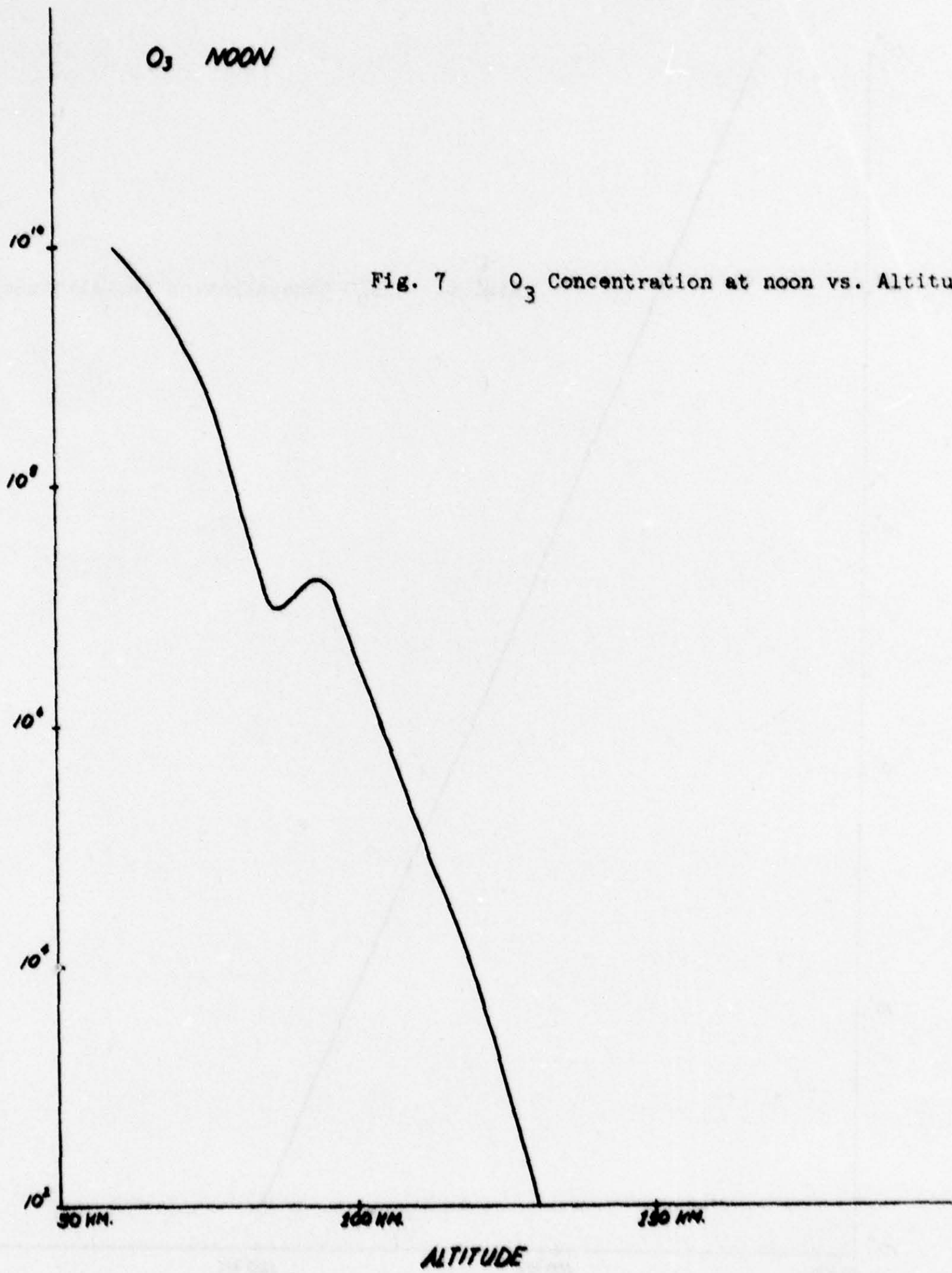


Fig. 7 $O_3$ Concentration at noon vs. Altitude

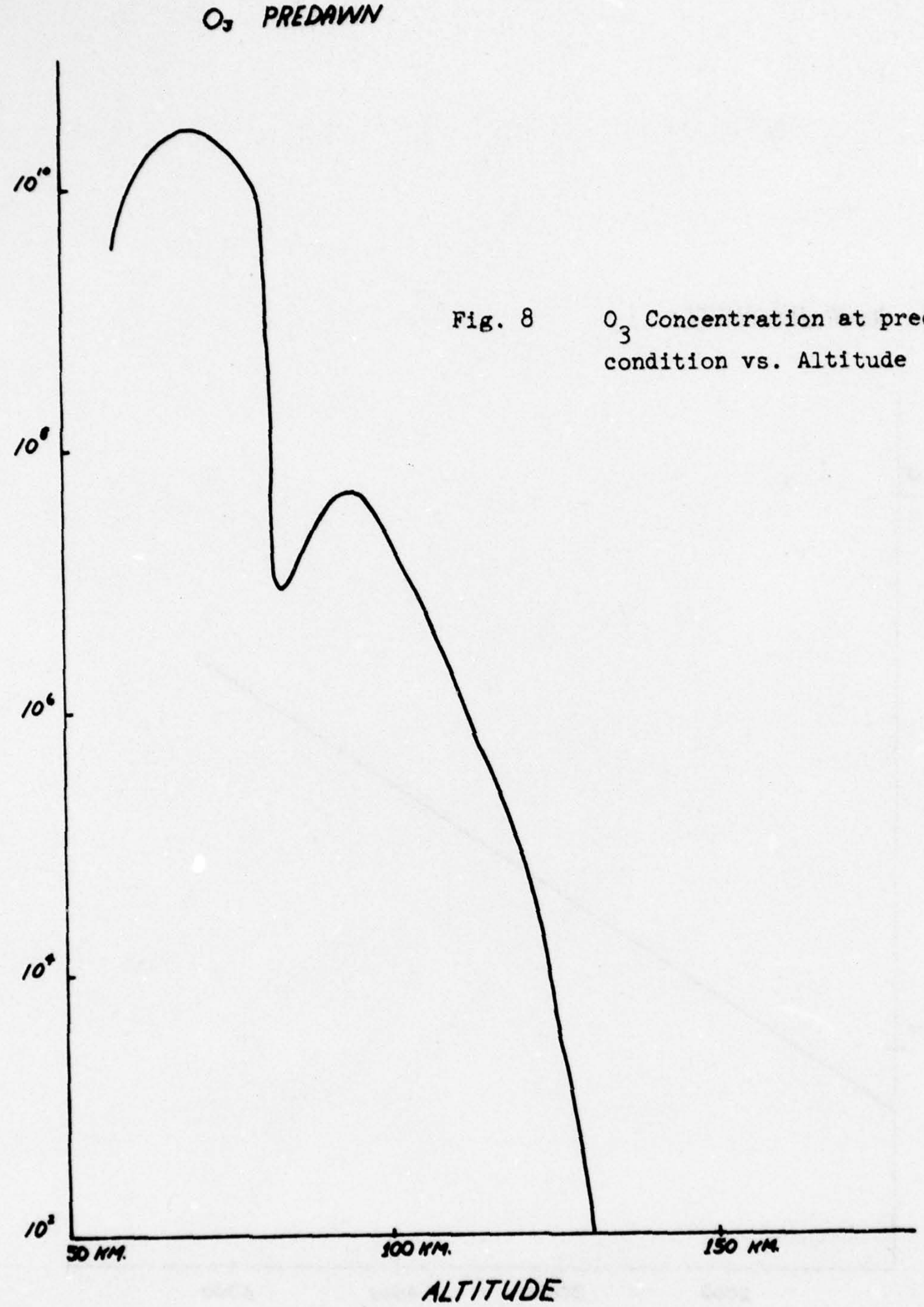


Fig. 8 $O_3$ Concentration at predawn condition vs. Altitude

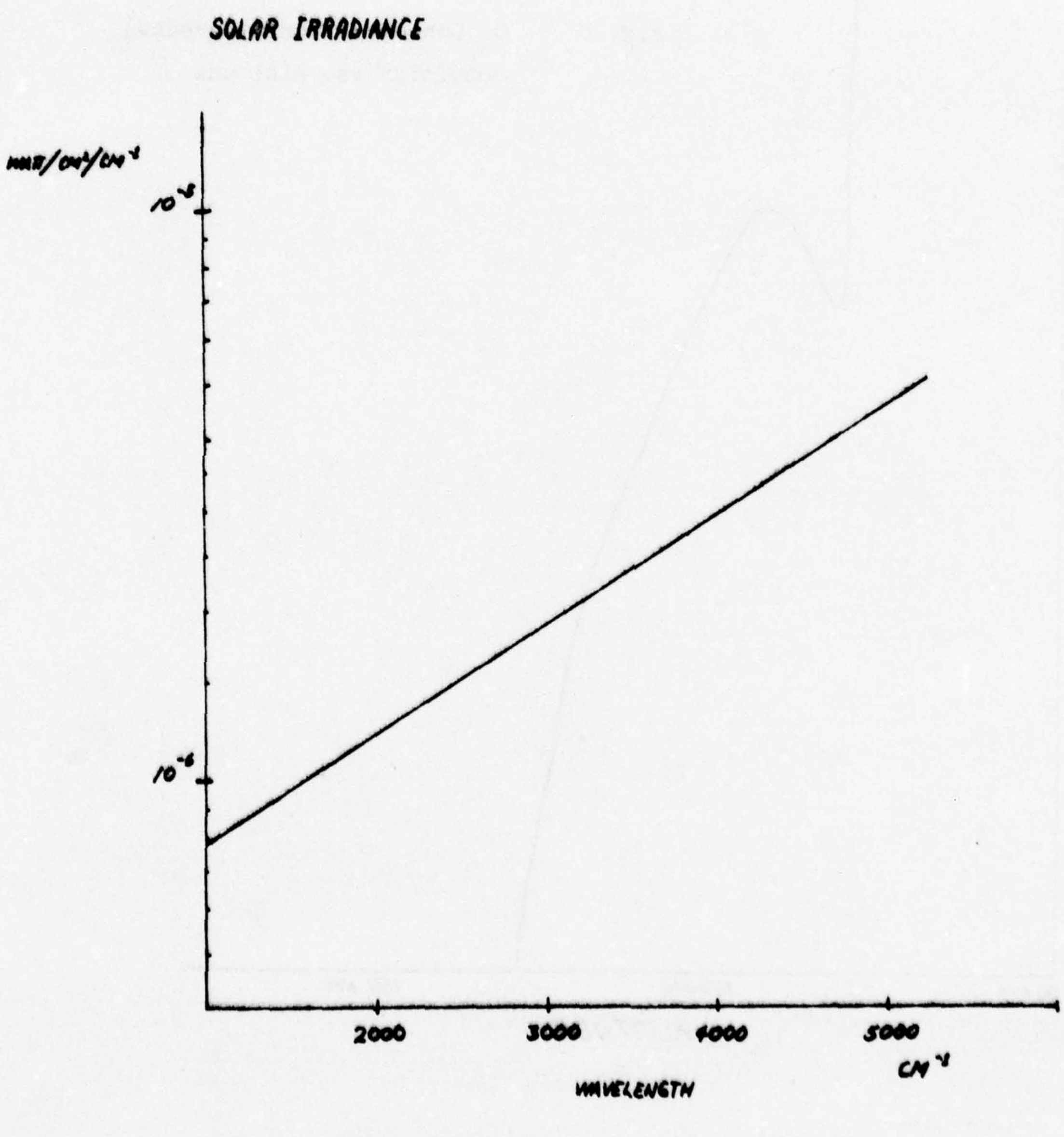


Fig. 9 Solar irradiance in watt/cm$^2$/cm$^{-1}$

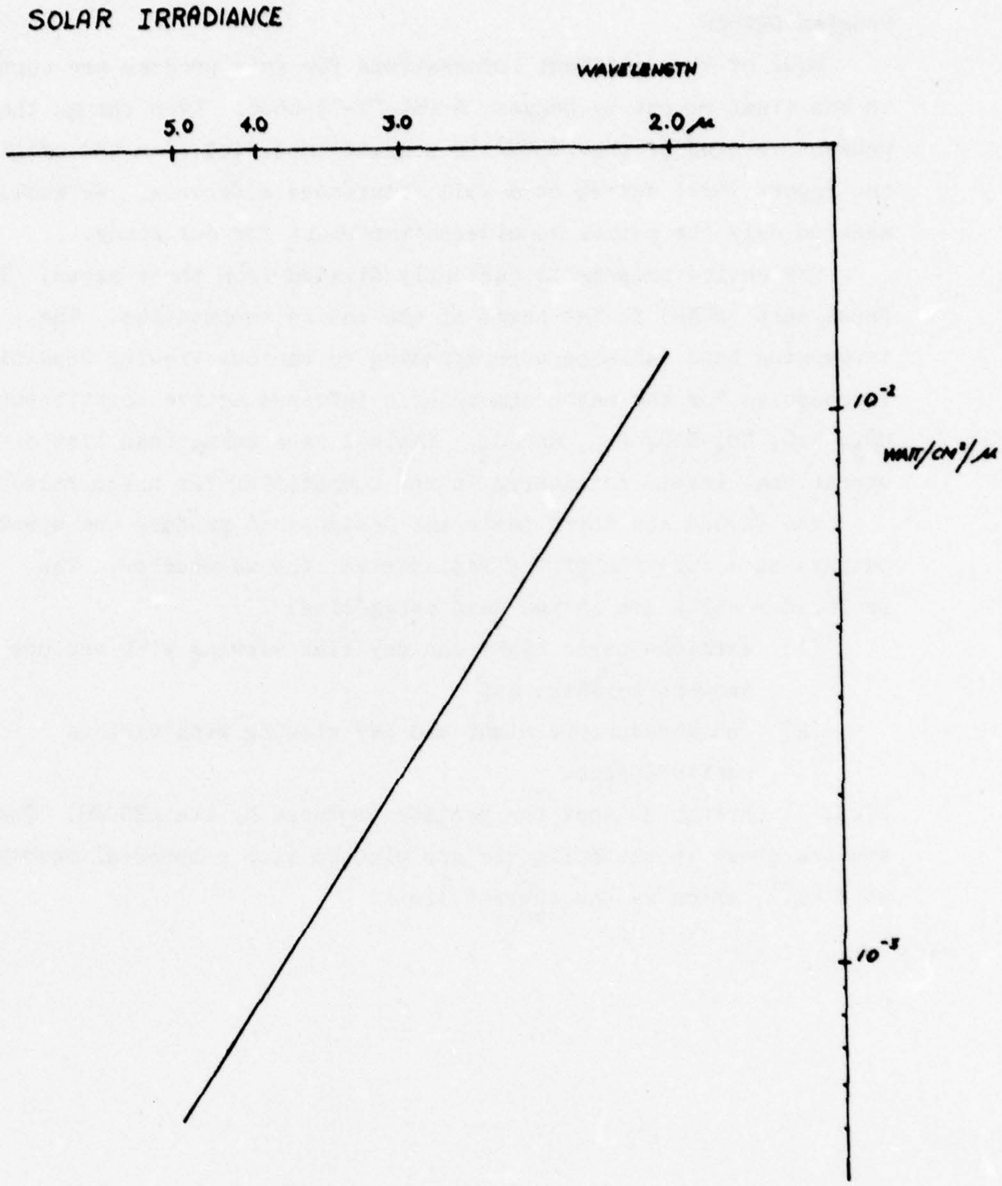


Fig. 10 Solar irradiance in watt/$cm^2$/μ

Program DEGGES

Most of the pertinent informations for this program are contained in the final report by Degges, AFCRL-TR-74-0606. Even though the present version of the DEGGES is somewhat modified from the original, the report still serves as a well documented reference. We shall mention only the points considered important for our study.

The entire program is currently divided into three parts. The first part (BGND) is the heart of the entire computation. The integrated band radiance corresponding to various viewing conditions is computed for the major atmospheric infrared active constituents: $CO_2$, $H_2O$, NO, $N_2O$, $CH_4$, and $O_3$. Table I is a summarized list of the vibrational levels considered in the computation for these molecules.

The second and third parts are designed to produce the spectral outputs as a function of the radiance vs. the wavenumber. The produced results are in two main categories:

(1) exoatmospheric night and day limb viewing with various tangent heights; and

(2) endoatmospheric night and day viewing with various zenith angles.

Figs. 11 through 34 show the results produced by the DEGGES. The spectra shown in these figures are plotted with a spectral resolution of 2 $cm^{-1}$, which is the current limit.

Table I

Vibrational Levels Included in the DEGGES Computation

$CO_2$

| | |
|---|---|
| 00001 | 0000.00 $cm^{-1}$ |
| 01101 | 667.38 |
| 10002 | 1285.41 |
| 02201 | 1335.13 |
| 10001 | 1388.19 |
| 11102 | 1932.47 |
| 03301 | 2003.30 |
| 00011 | 2349.15 |
| 10012 | 3612.84 |
| 10011 | 3714.78 |

$H_2O$

| | |
|---|---|
| 000 | 0000.00 $cm^{-1}$ |
| 010 | 1594.74 |
| 020 | 3151.63 |
| 100 | 3657.05 |
| 001 | 3755.92 |
| 030 | 4666.72 |
| 110 | 5234.98 |
| 011 | 5331.25 |

Table I (Continued)

| | | |
|---|---|---|
| $N_2O$ | | |
| | 0000 | 0000.00 $cm^{-1}$ |
| | 0110 | 588.8 |
| | or 0200) 0220) | 1173.0 |
| | 0310 | 1758.3 |
| | or 0400) 0420) | 2338.5 |
| | 0001 | 2223.5 |
| | 1000 | 1285.0 |
| NO | | |
| | v = 0 | 0000.00 $cm^{-1}$ |
| | v = 1 | 1878.0 |
| | v = 2 | 3727.0 |
| $O_3$ | | |
| | 000 | 000.00 $cm^{-1}$ |
| | 001 | 1042.1 |
| $CH_4$ | | |
| | 00000000 | 0000.00 $cm^{-1}$ |
| | 00000111 | 1306.2 |
| | 01100001 | 1526.0 |
| | 00011001 | 3018.4 |

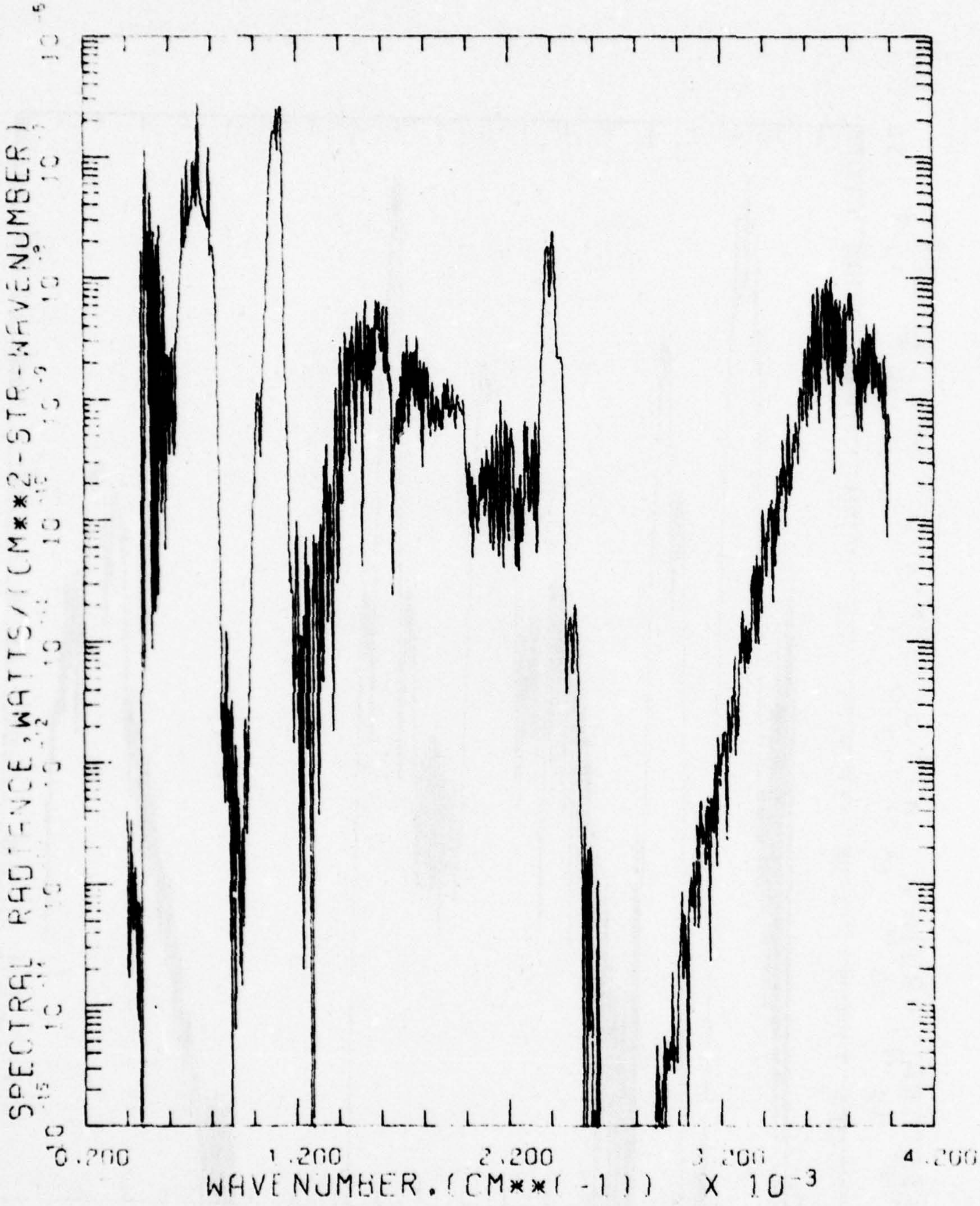


Fig. 11 Day Limb Viewing Radiance at 60 Km Tangent Height.

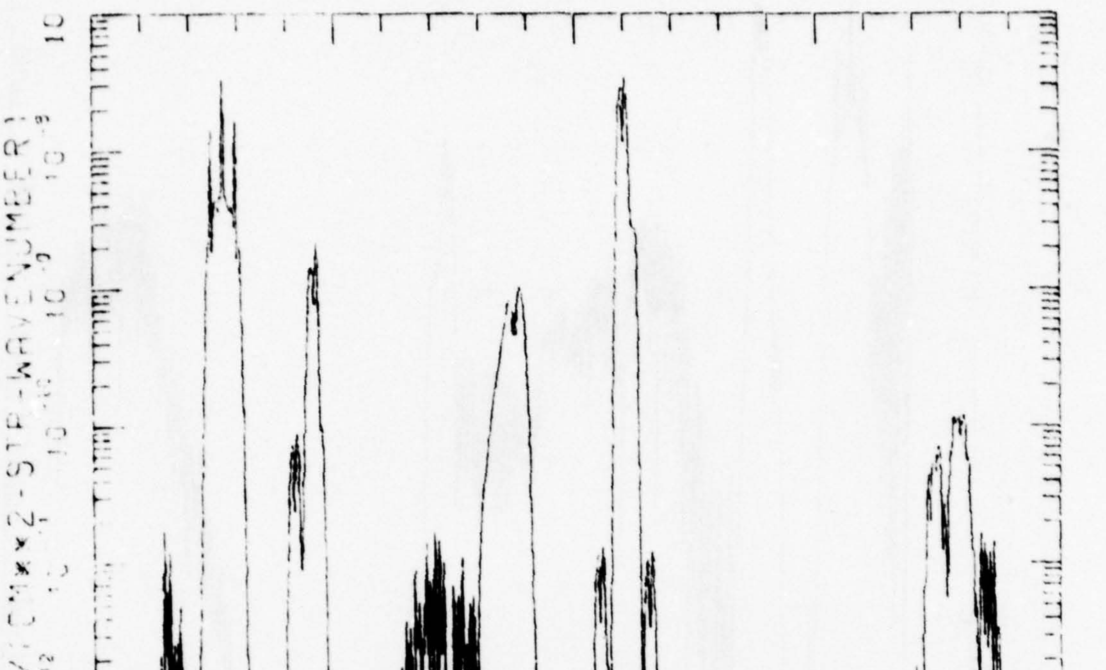


Fig. 12 Day Limb Viewing Radiance at 80 Km Tangent Height.

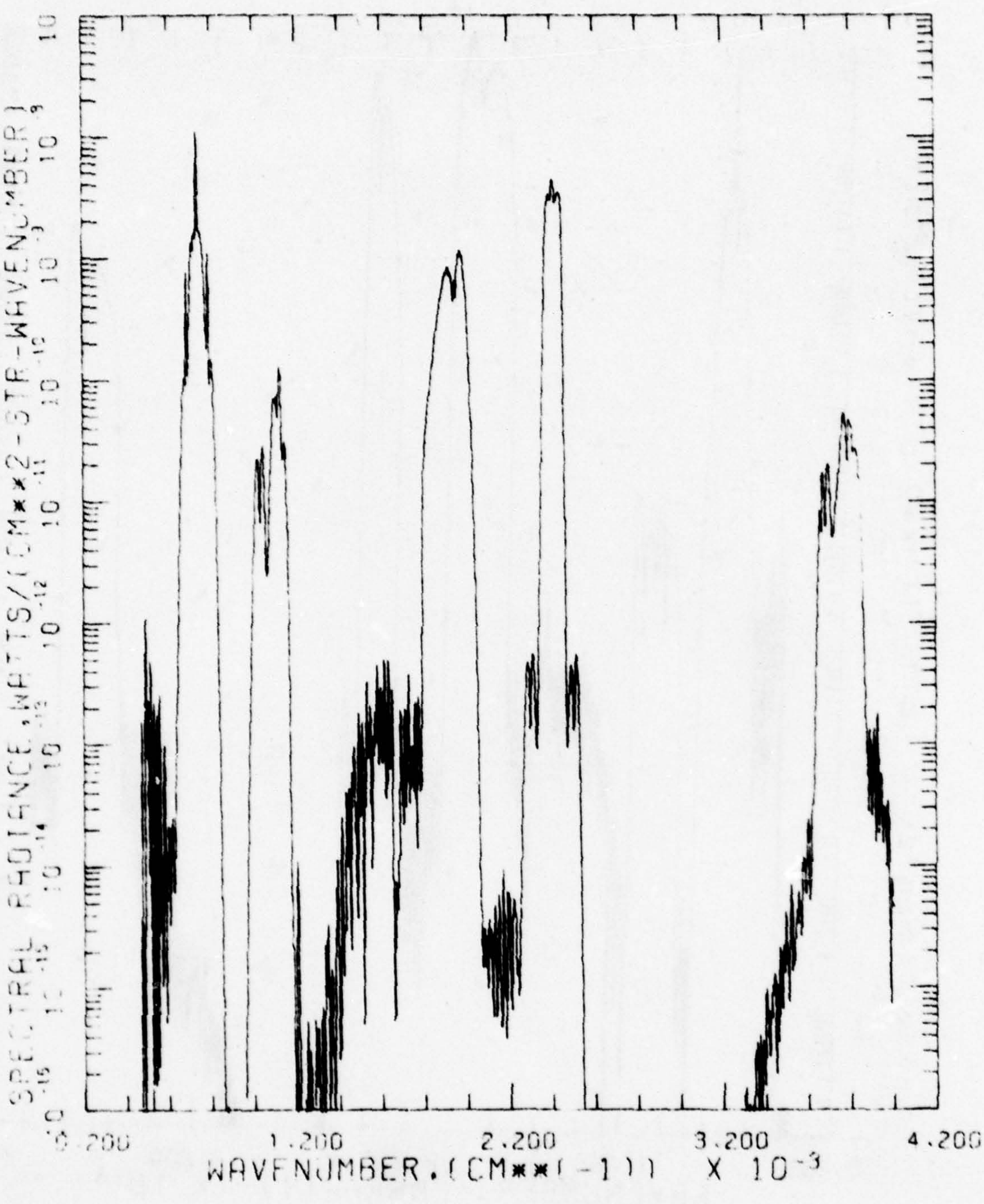


Fig. 13 Day Limb Viewing at 100 Km Tangent Height.

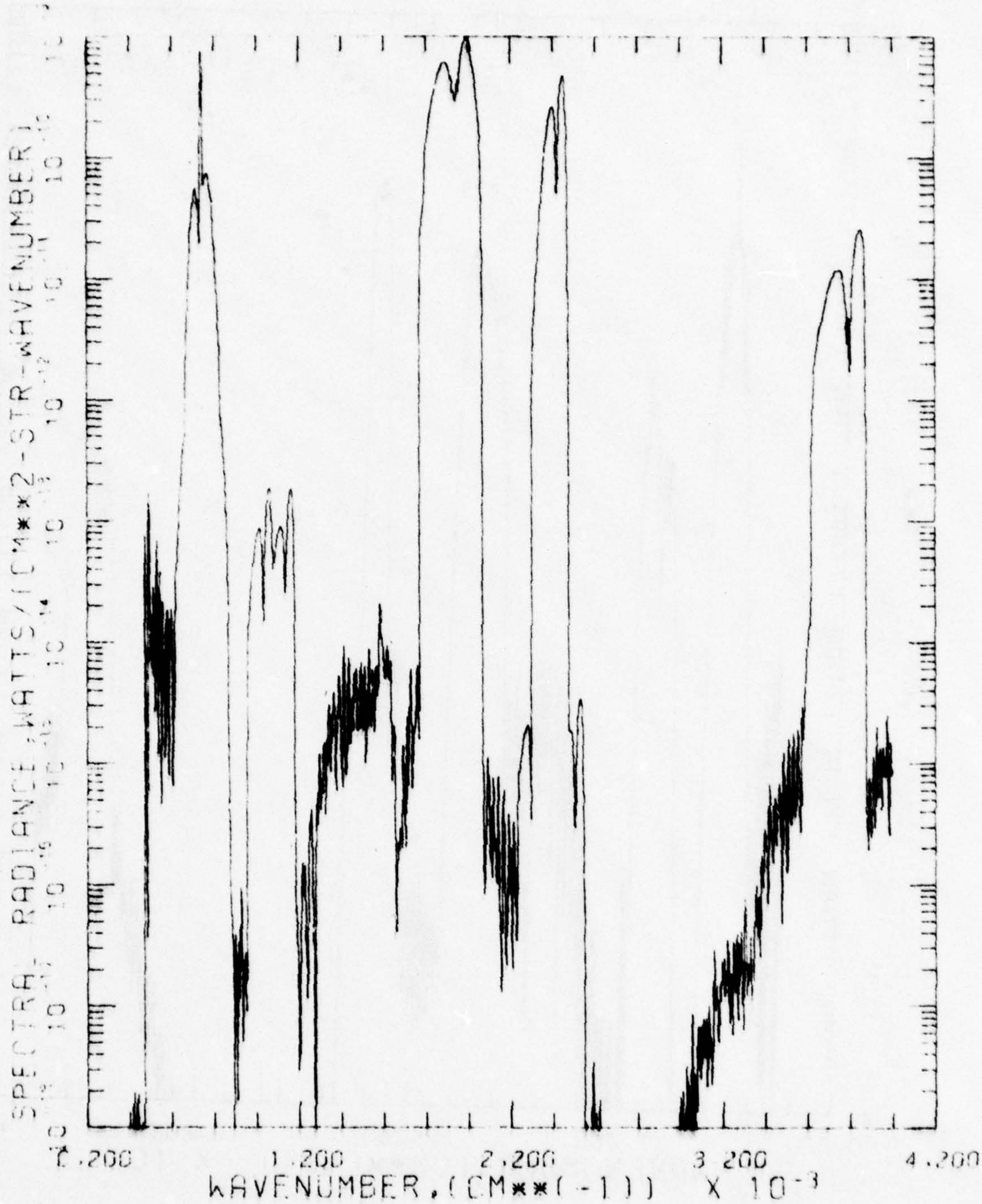


Fig. 14 Day Limb Viewing Radiance at 150 Km Tangent Height.

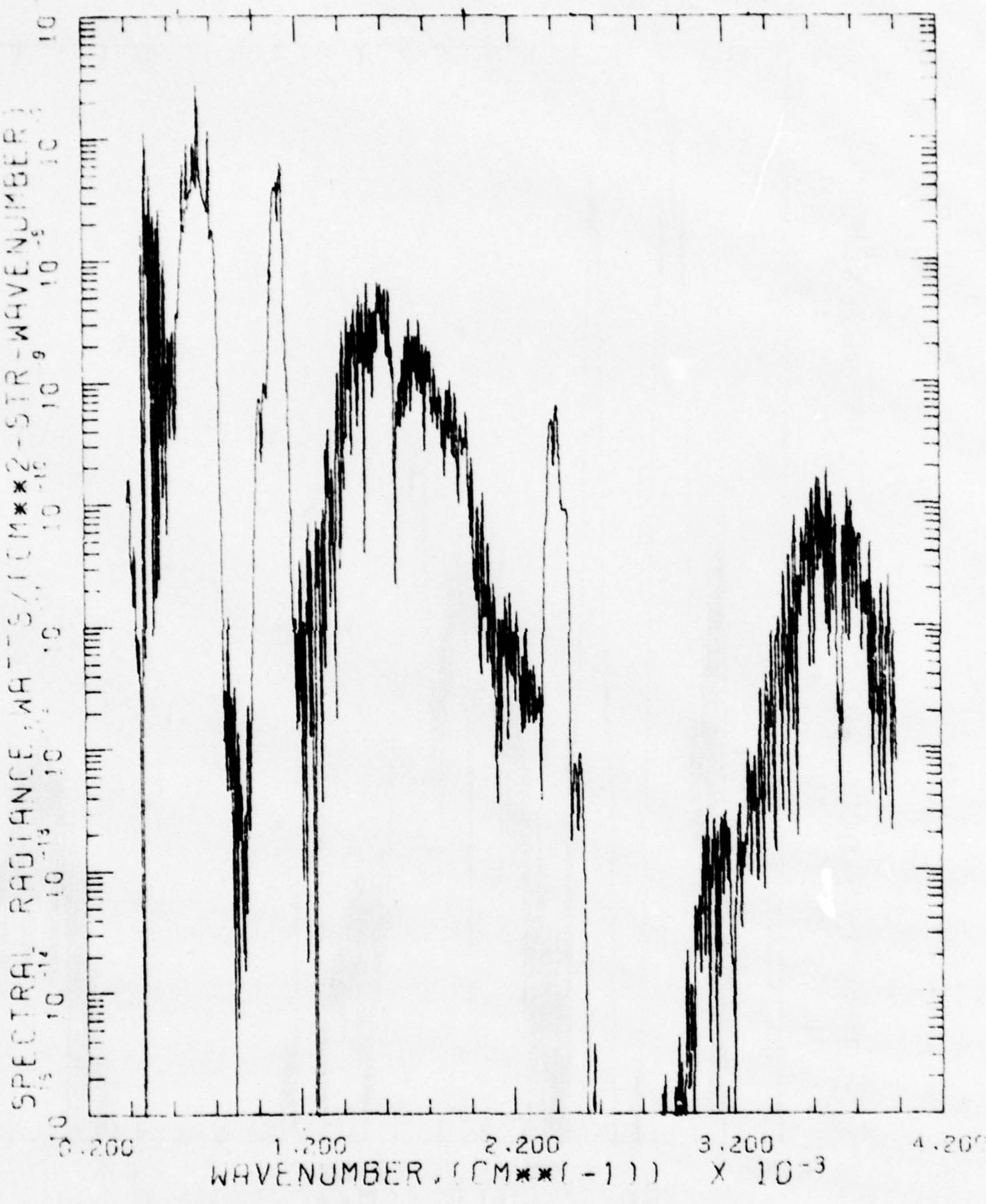


Fig. 15 Night Limb Viewing Radiance at 60 Km Tangent Height.

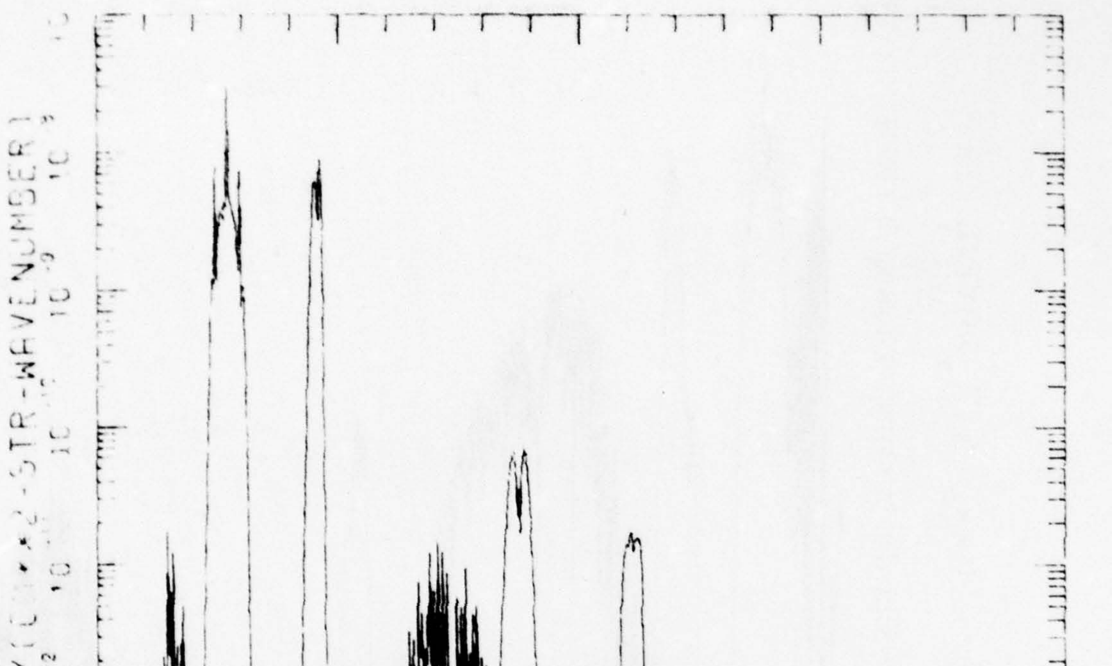


Fig. 16 Night Limb Viewing Radiance at 80 Km Tangent Height.

ALTITUDE

9

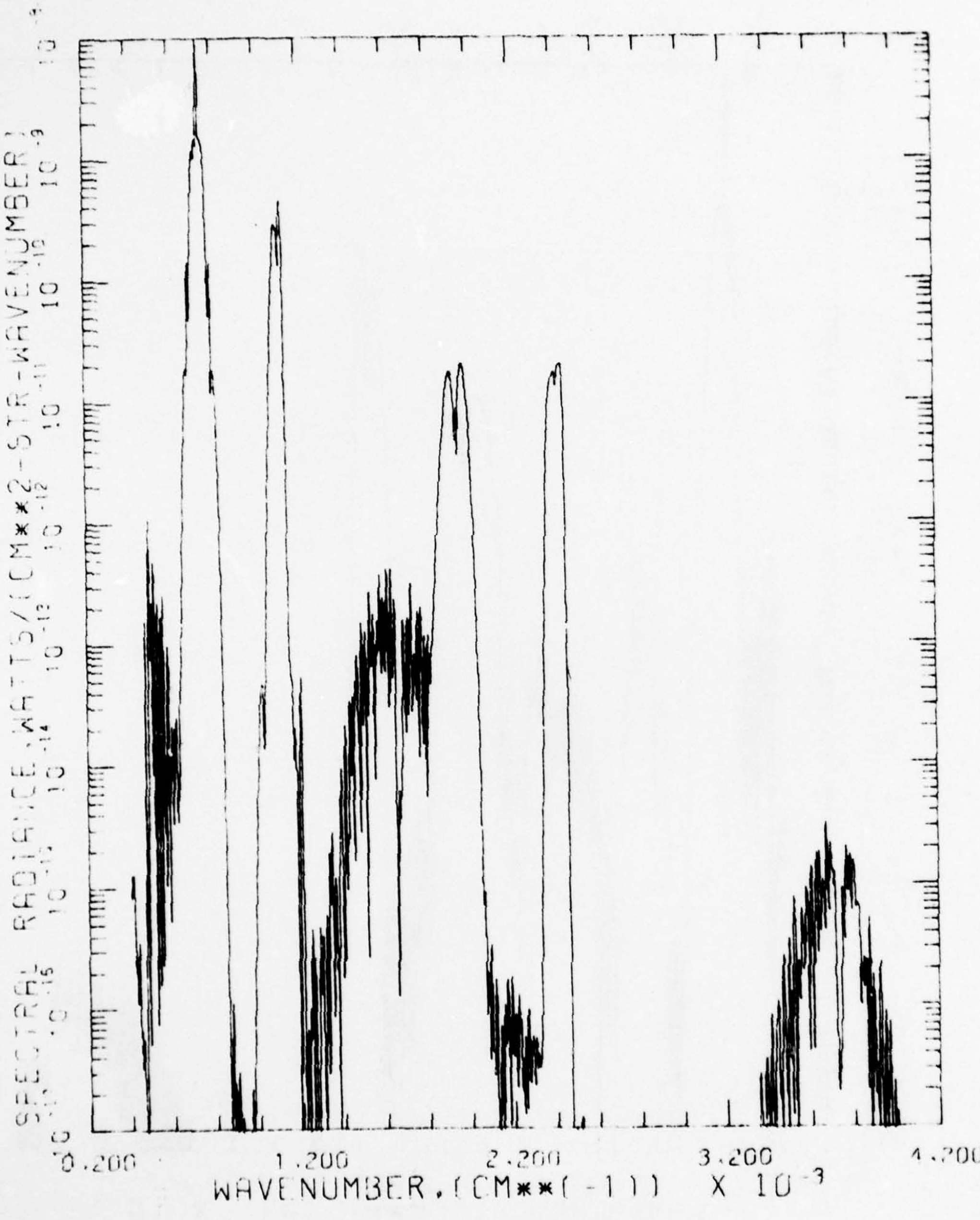


Fig. 17 Night Limb Viewing Radiance at 100 Km Tangent Height.

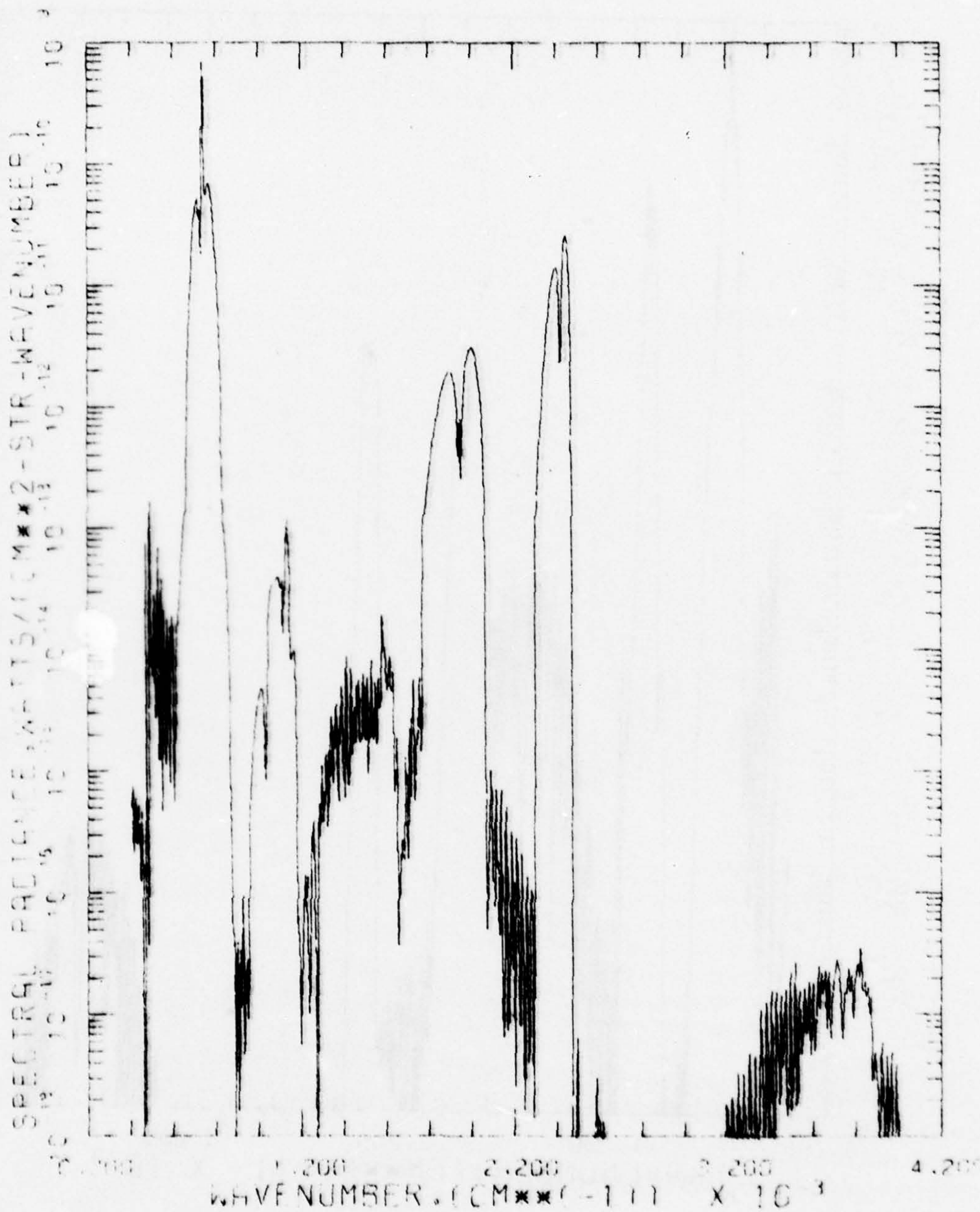


Fig. 18 Night Limb Viewing Radiance at 150 Km Tangent Height.

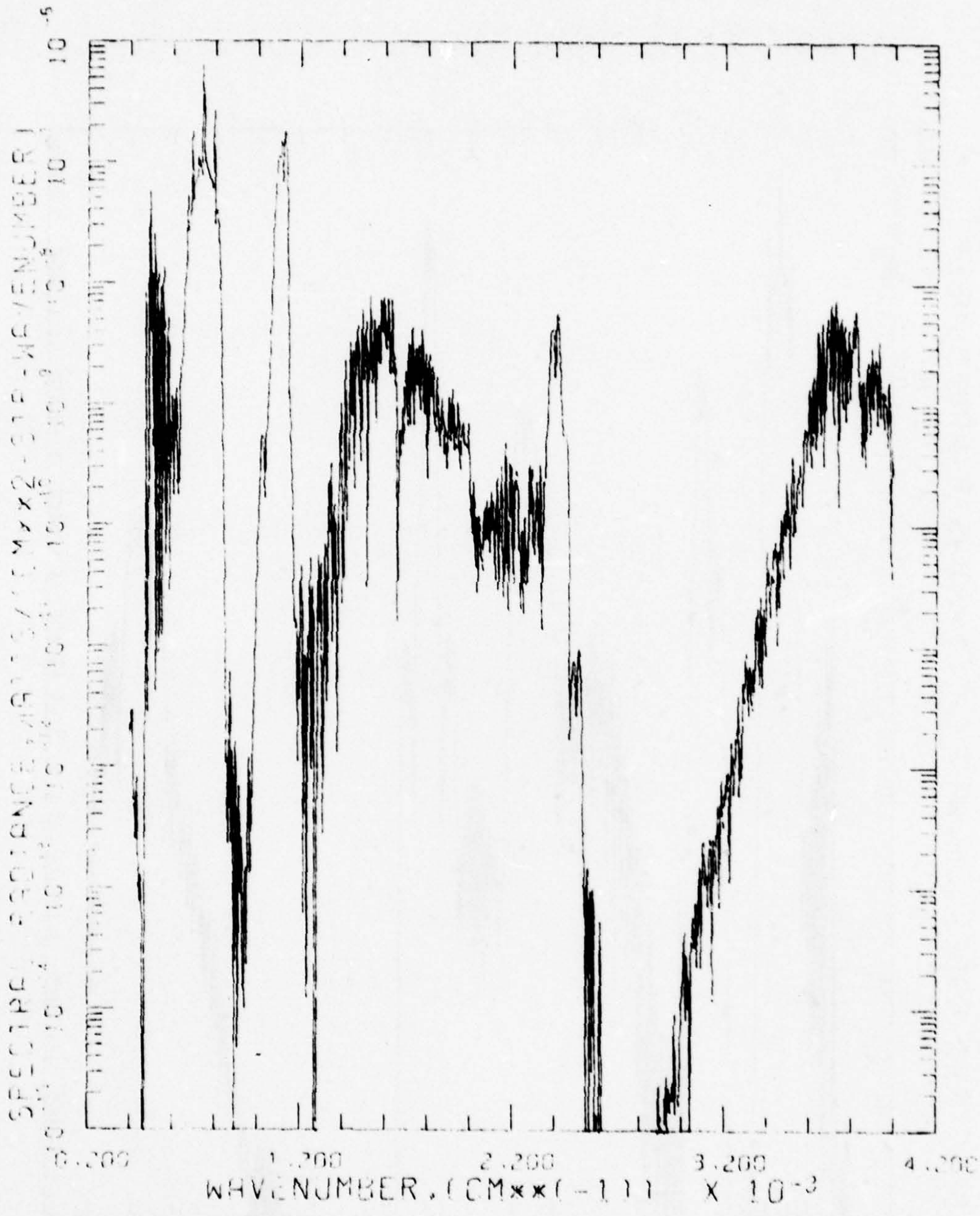


Fig. 19 Day Horizontal Viewing Radiance at 60 Km Altitude.

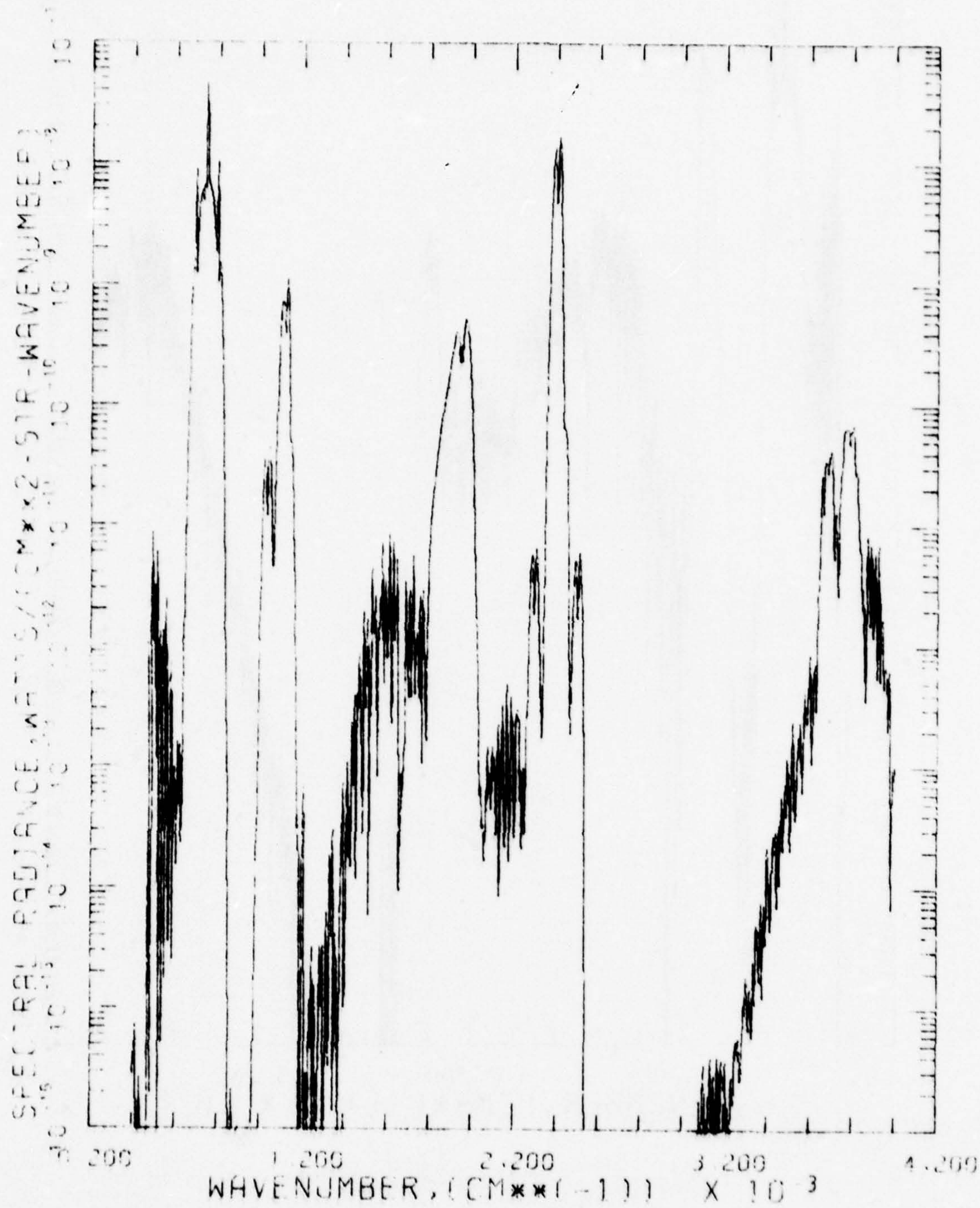


Fig. 20 Day Horizontal Viewing Radiance at 80 Km Altitude.

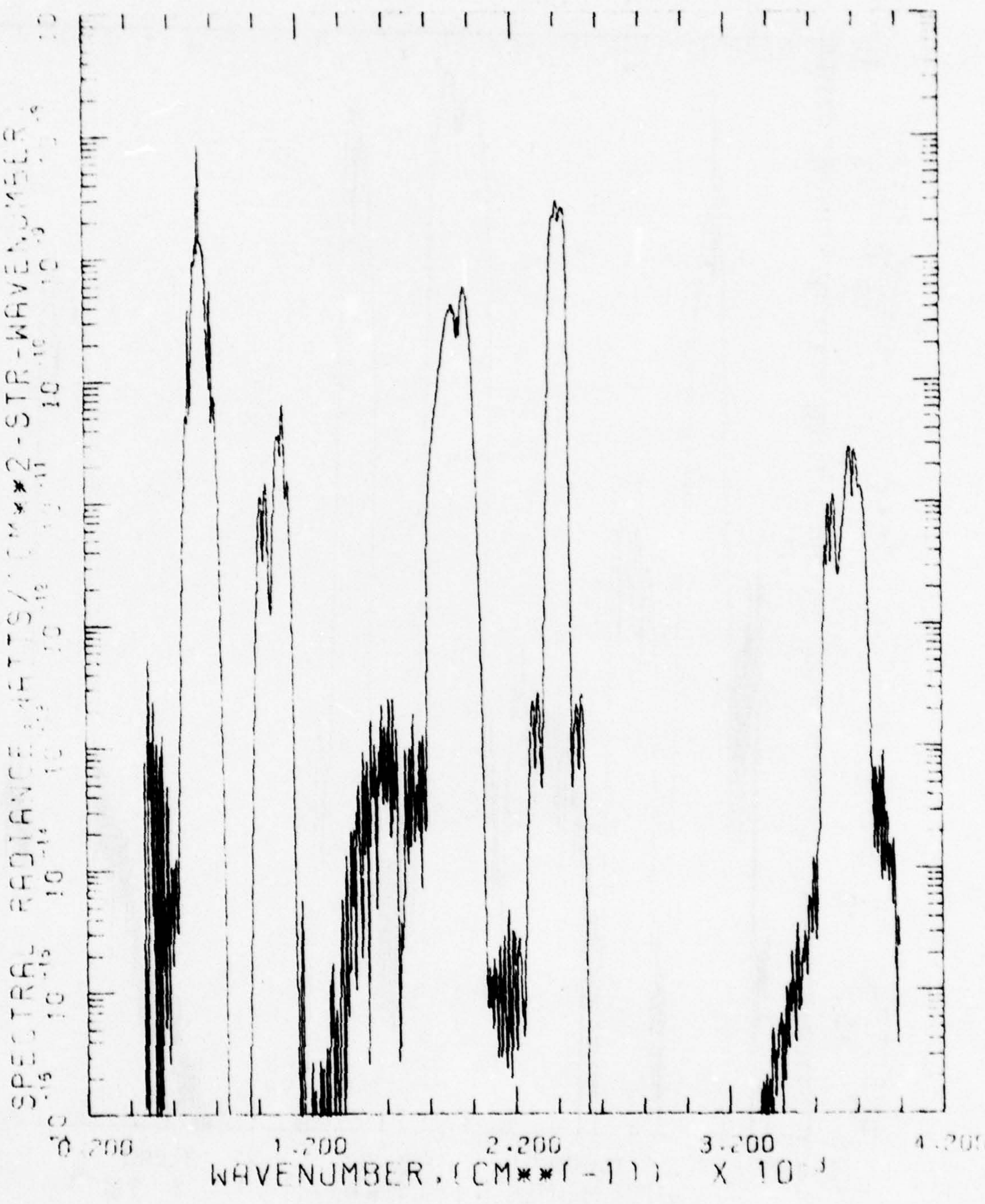


Fig. 21 Day Horizontal Viewing Radiance at 100 Km Altitude.

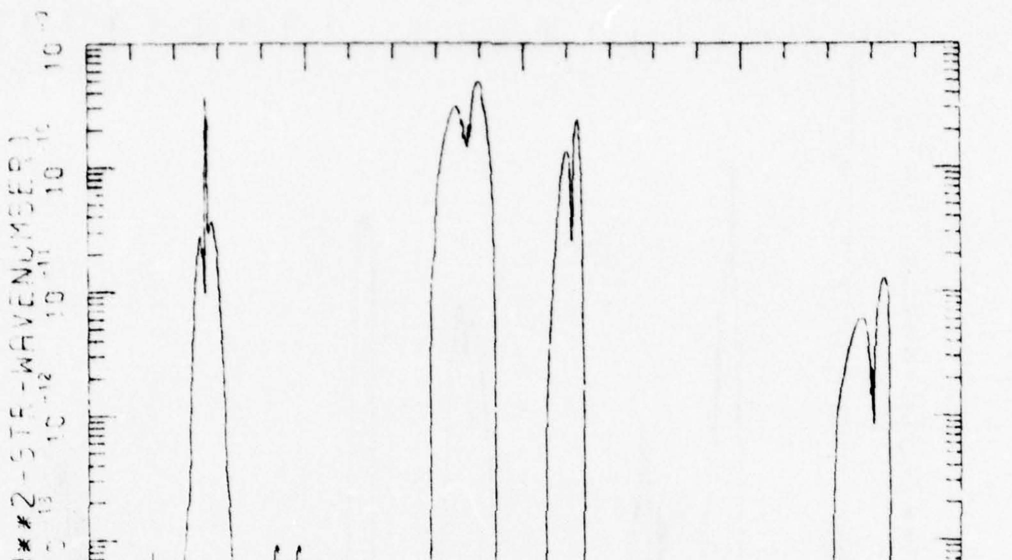


Fig. 22 Day Horizontal Viewing Radiance at 150 Km Altitude.

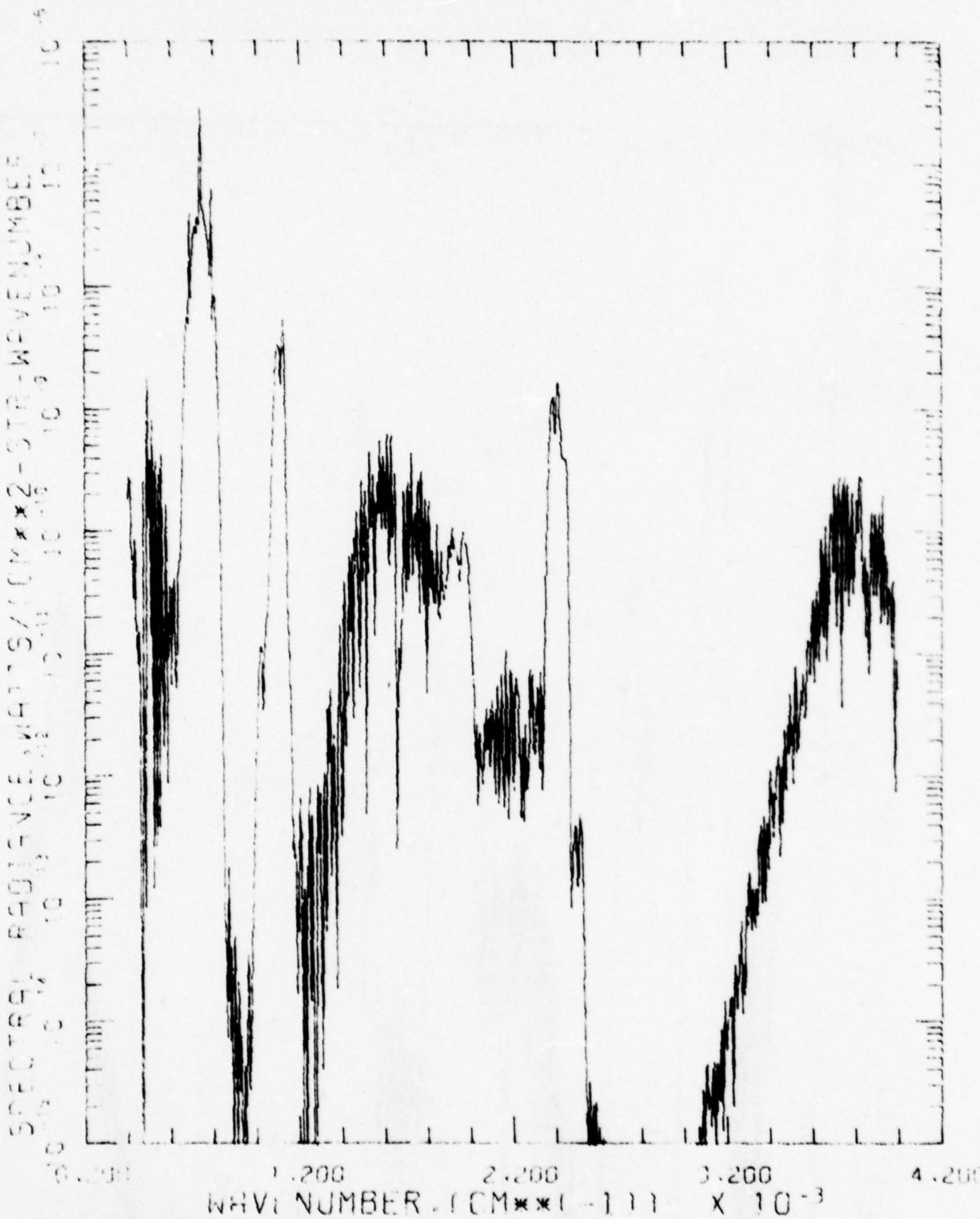


Fig. 23 Day Vertical Viewing Radiance at 60 Km Altitude.

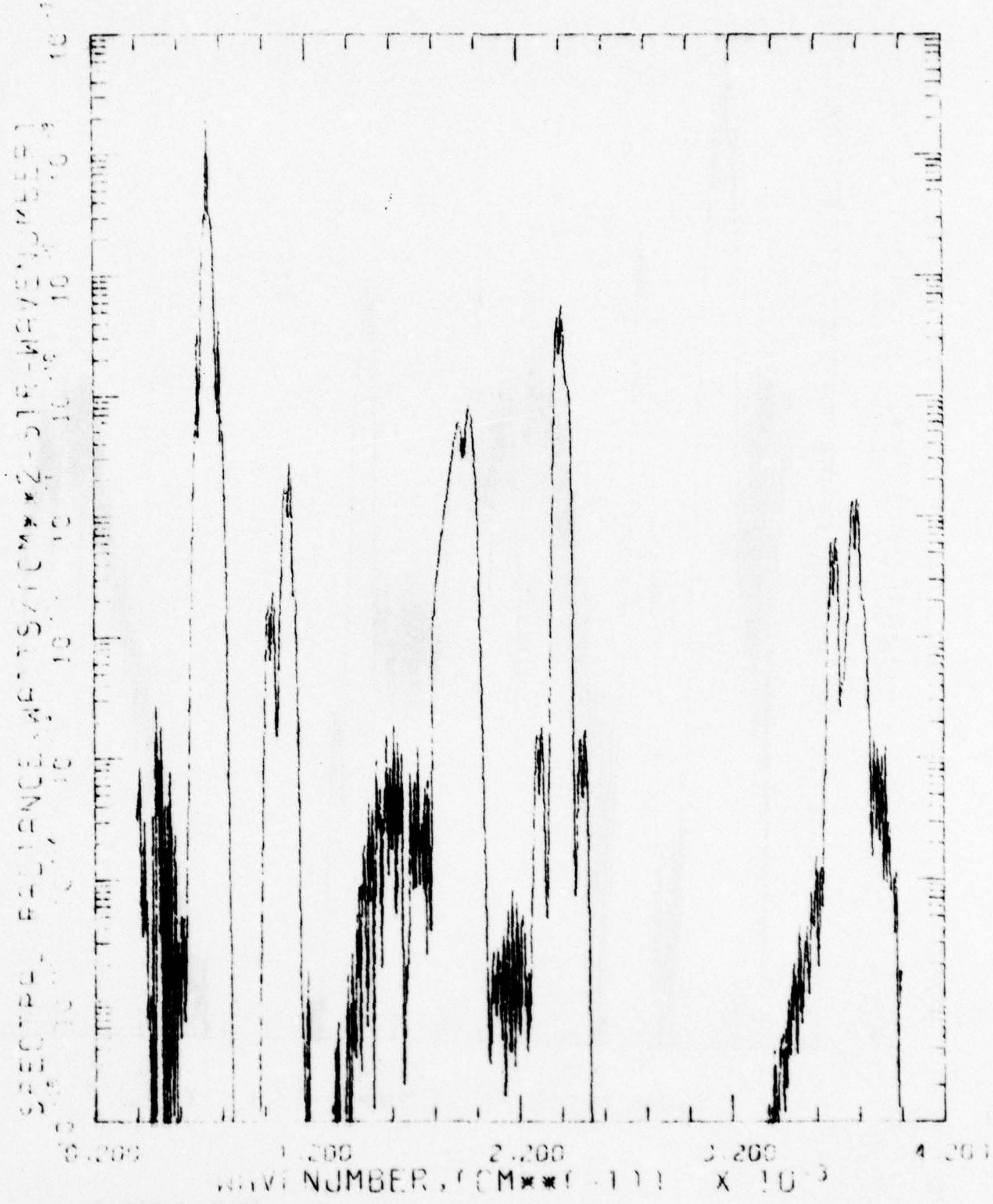

Fig. 24 Day Vertical Viewing Radiance at 80 Km Altitude.

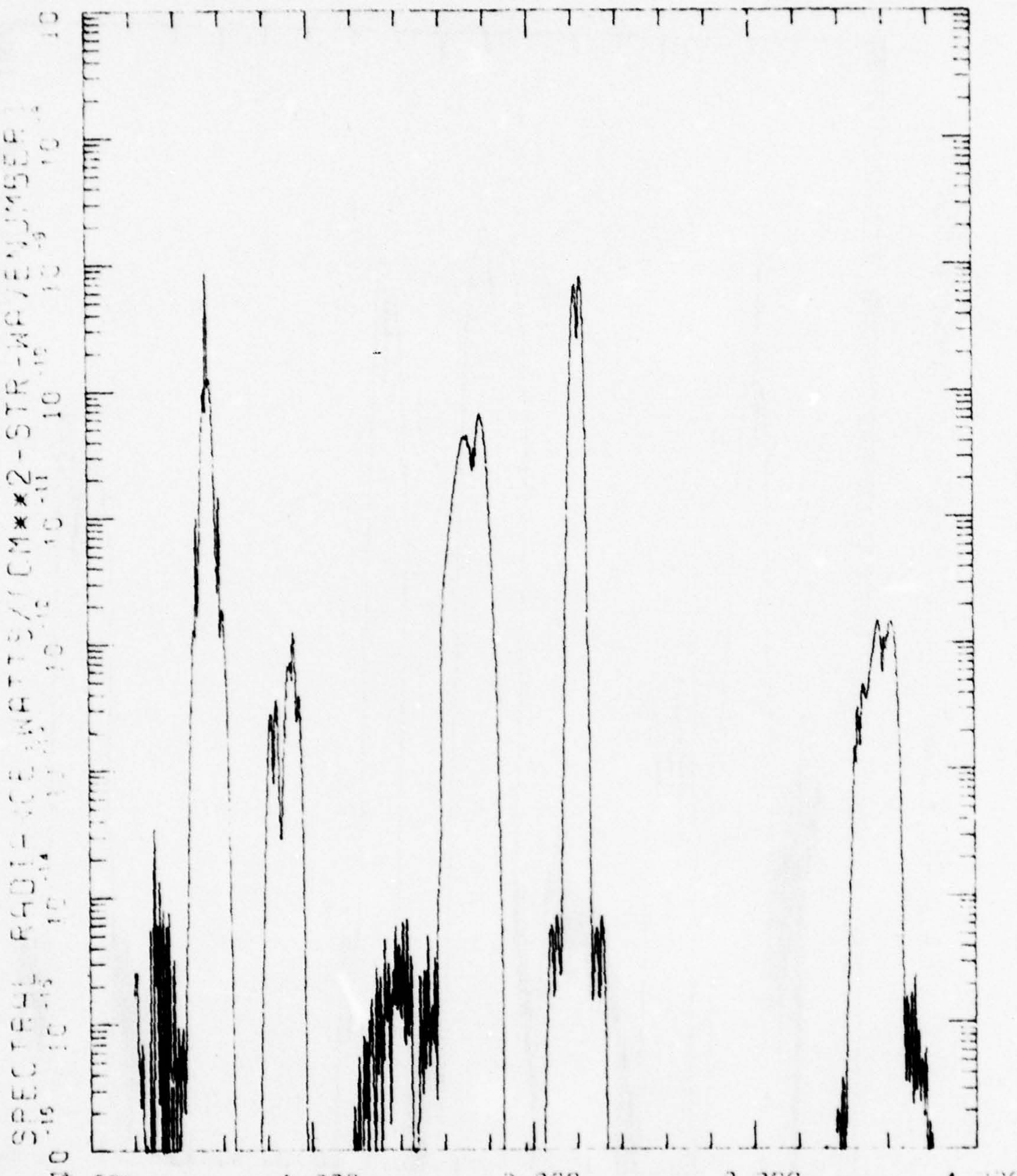


Fig. 25 Day Vertical Viewing Radiance at 100 Km Altitude.

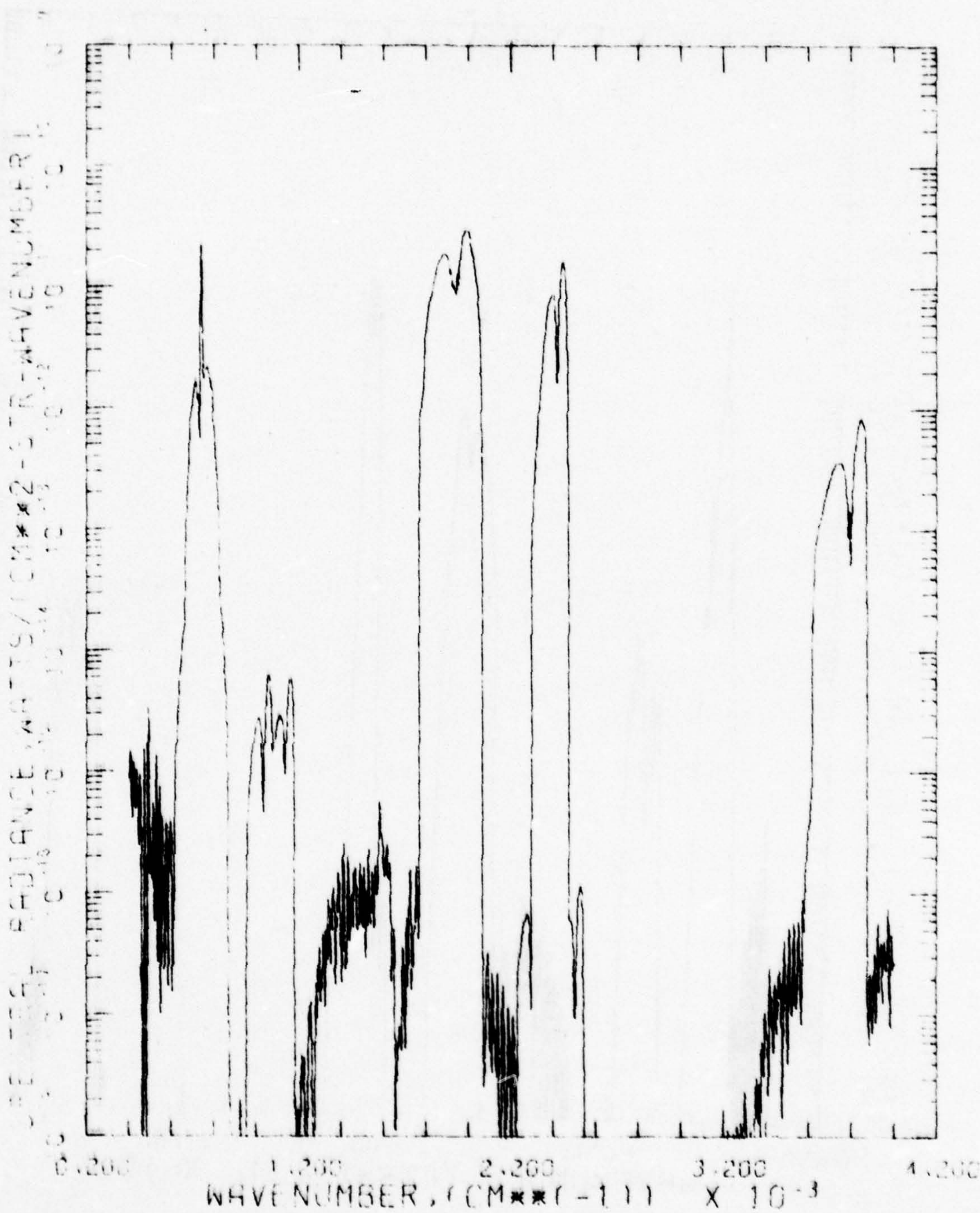


Fig. 26 Day Vertical Viewing Radiance at 150 Km Altitude.

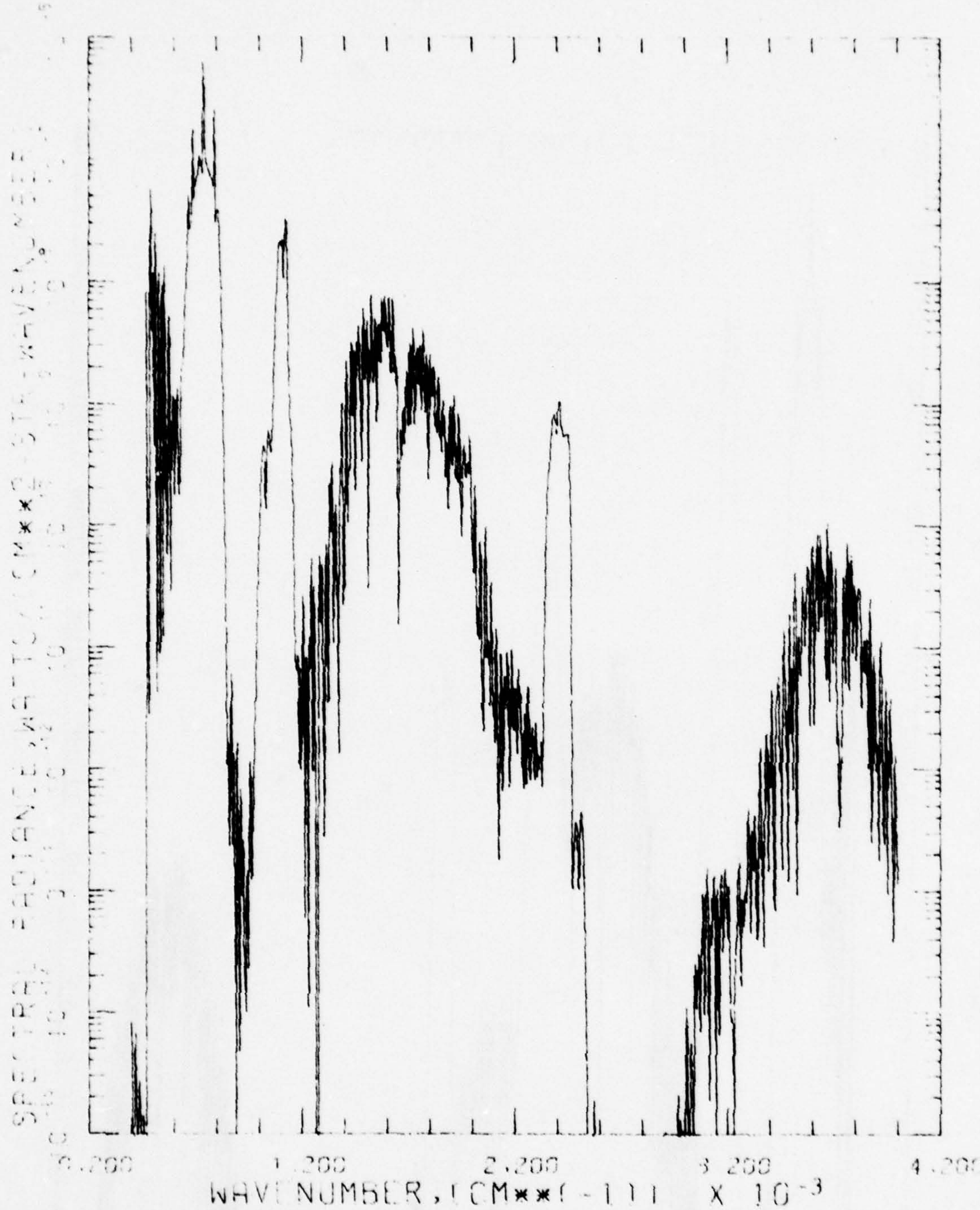


Fig. 27 Night Horizontal Viewing Radiance at 60 Km Altitude.

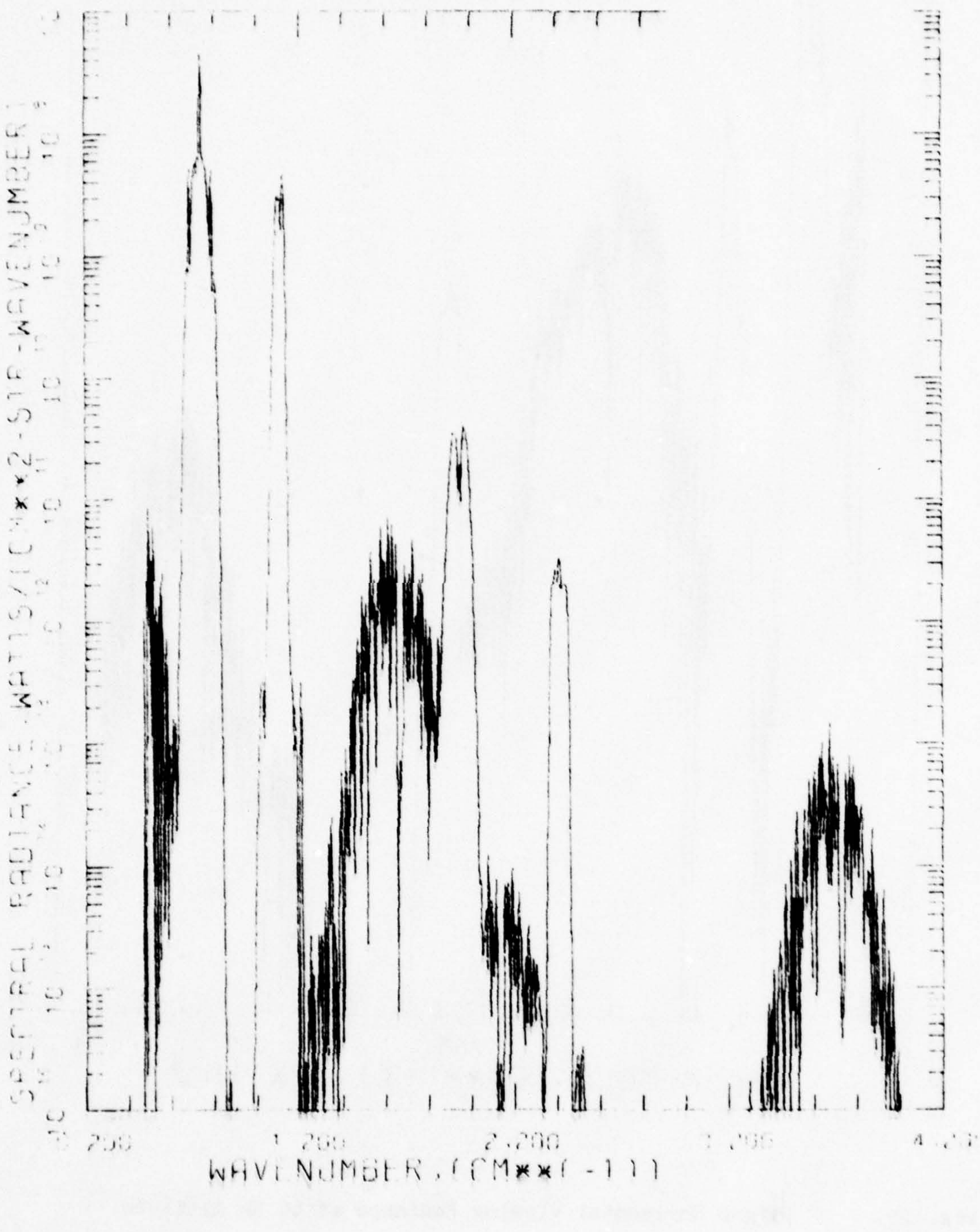


Fig. 28 Night Horizontal Viewing Radiance at 80 Km Altitude.

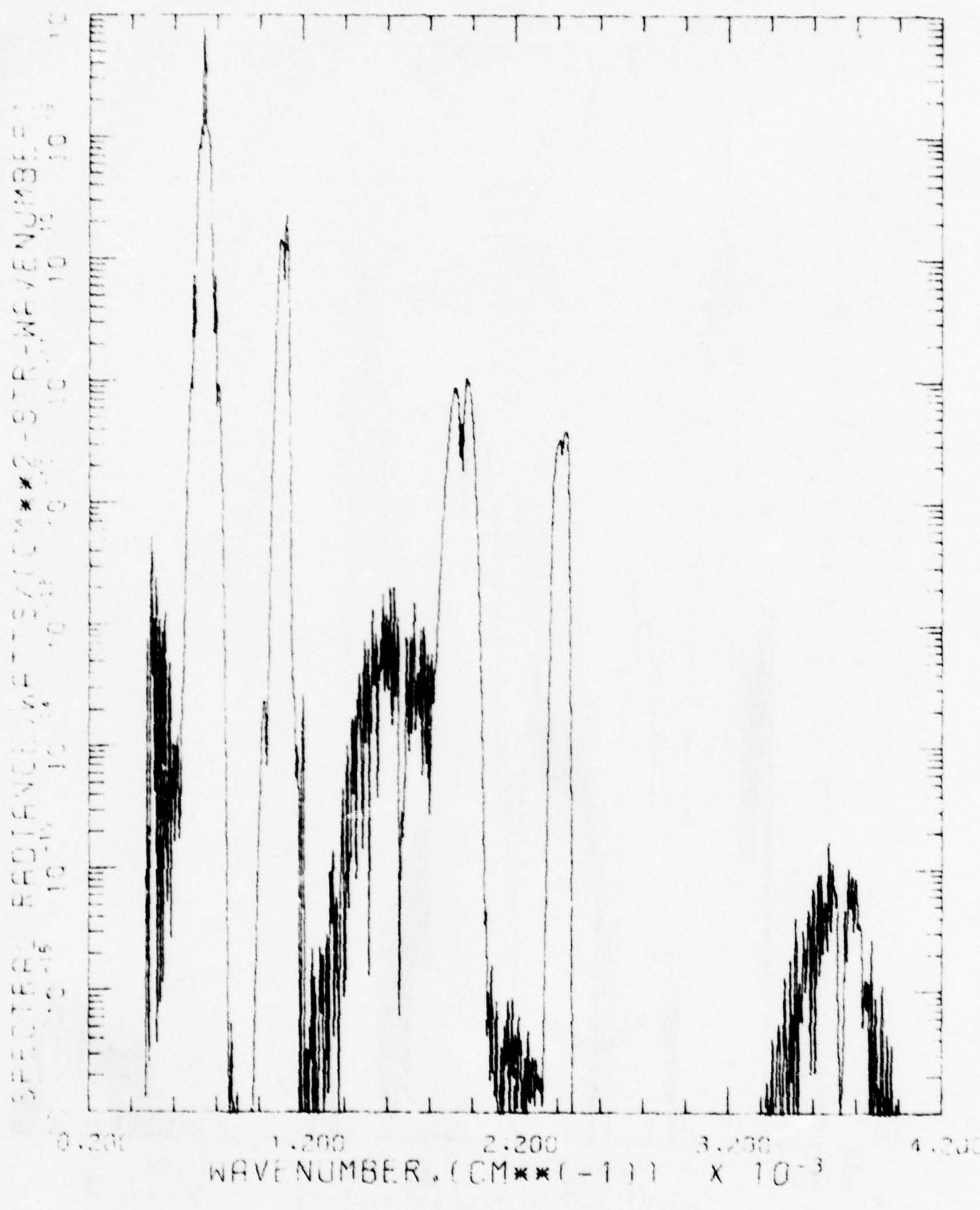


Fig. 29 Night Horizontal Viewing Radiance at 100 Km Altitude.

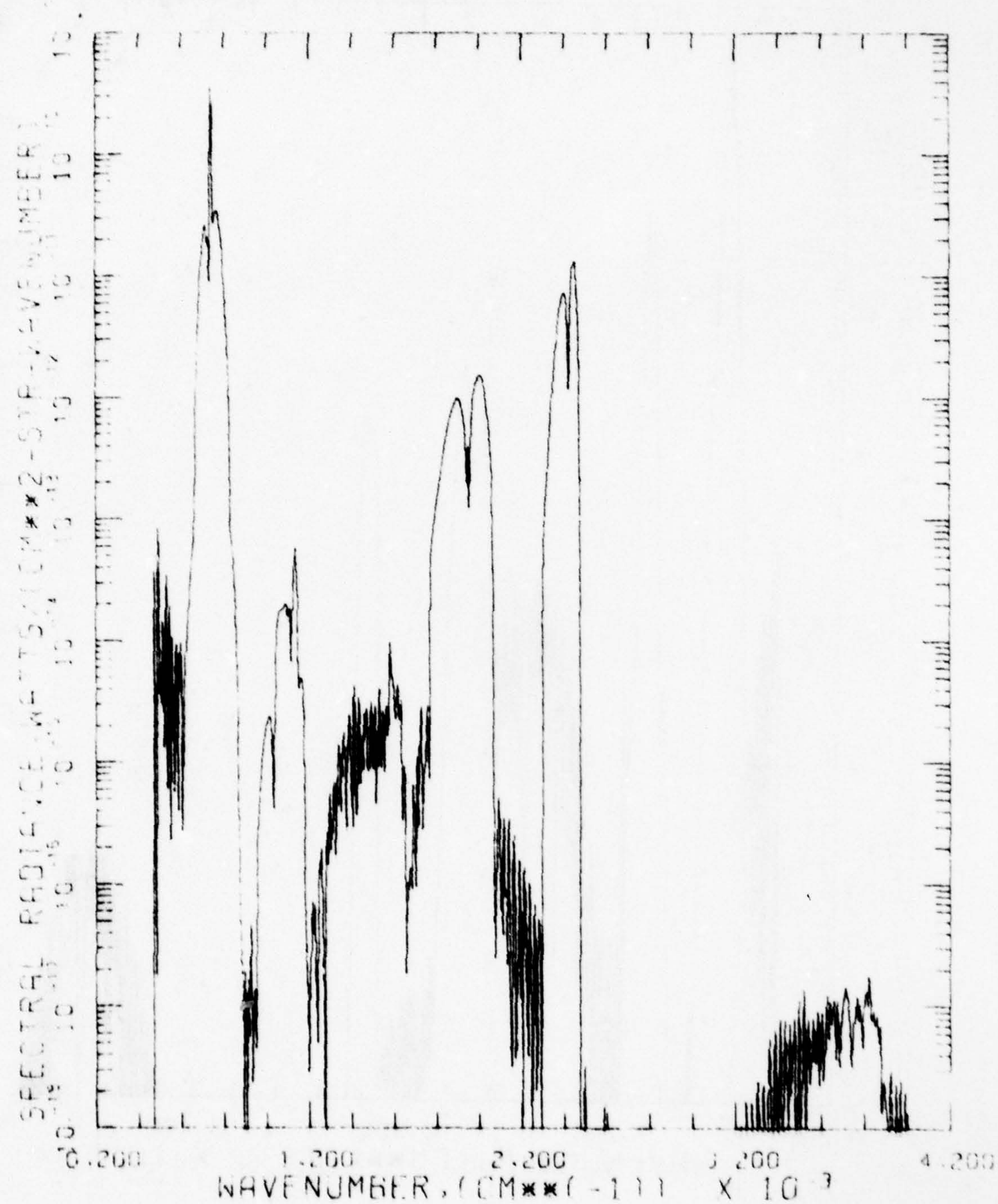


Fig. 30 Night Horizontal Viewing Radiance at 150 Km Altitude.

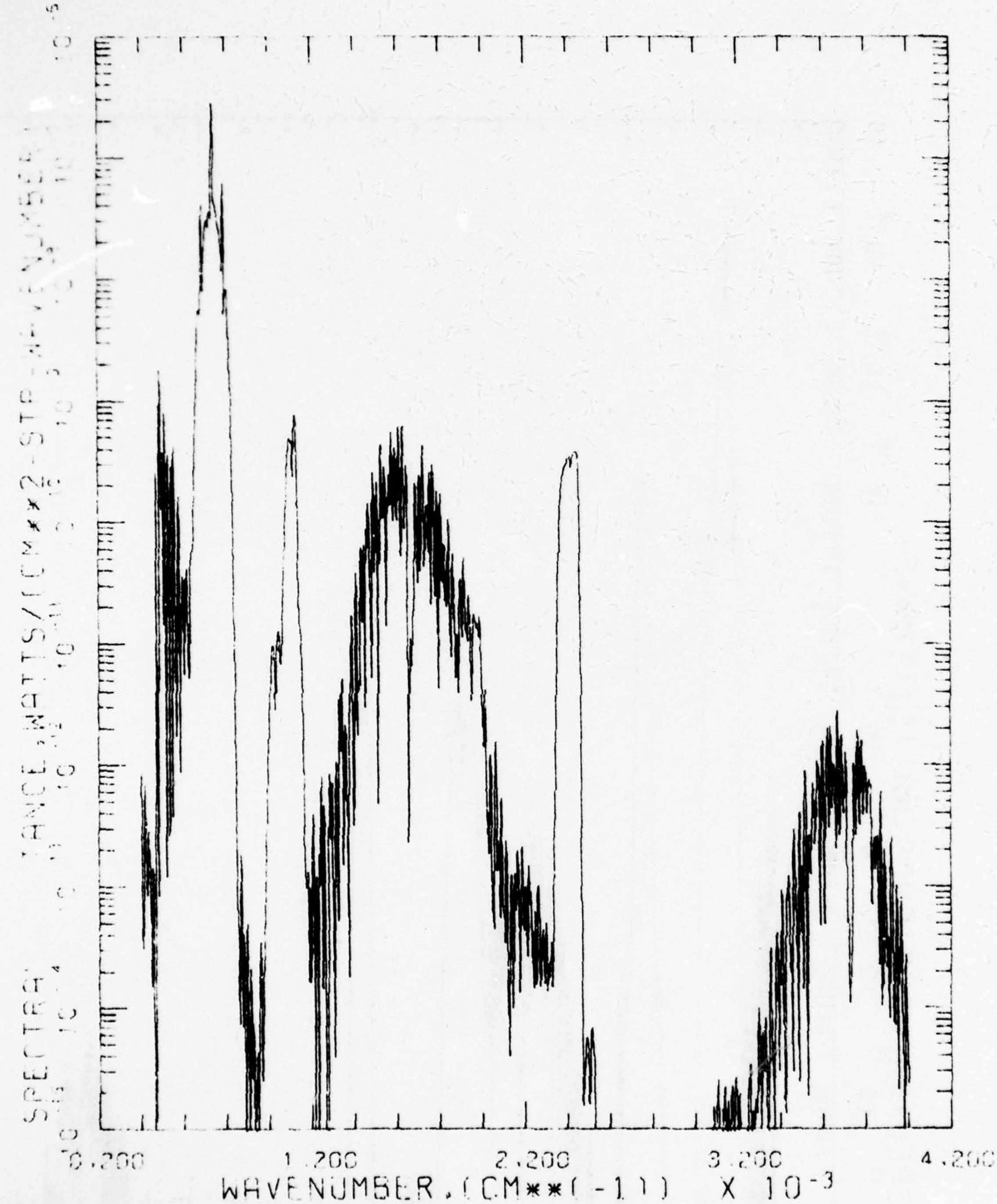


Fig. 31 Night Vertical Viewing Radiance at 60 Km Altitude.

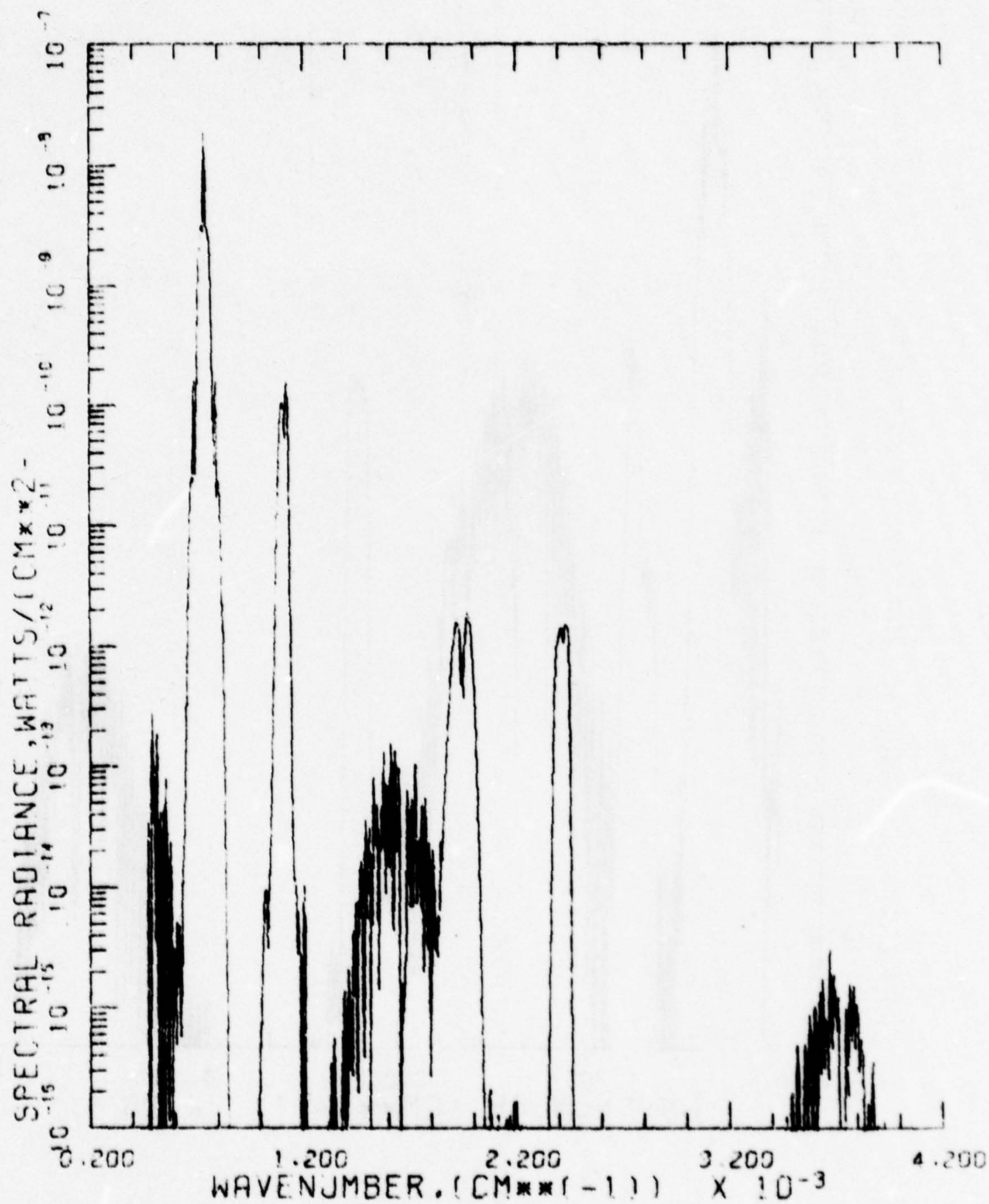


Fig. 32 Night Vertical Viewing Radiance at 80 Km Altitude.

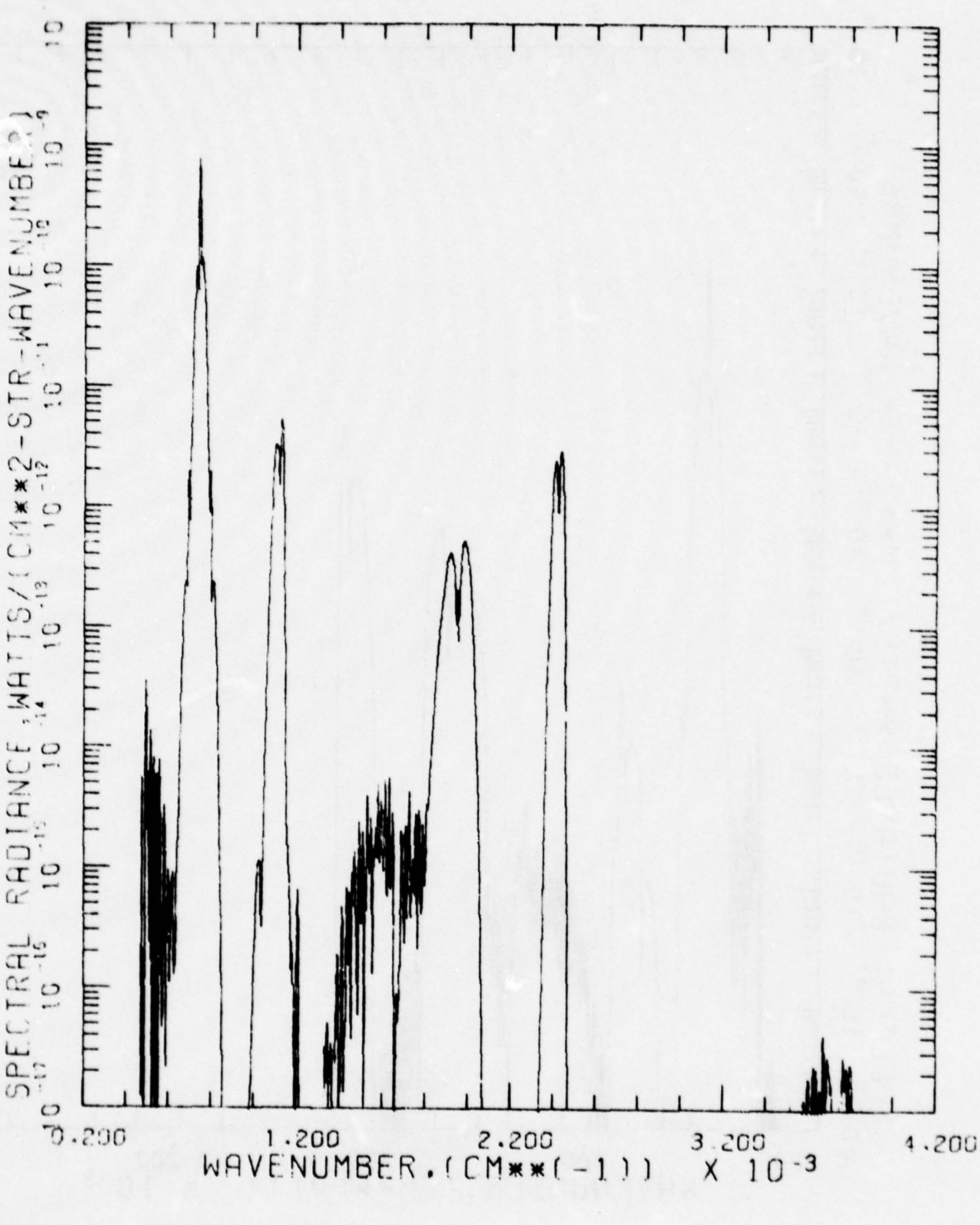


**Fig. 33 Night Vertical Viewing Radiance at 100 Km Altitude.**

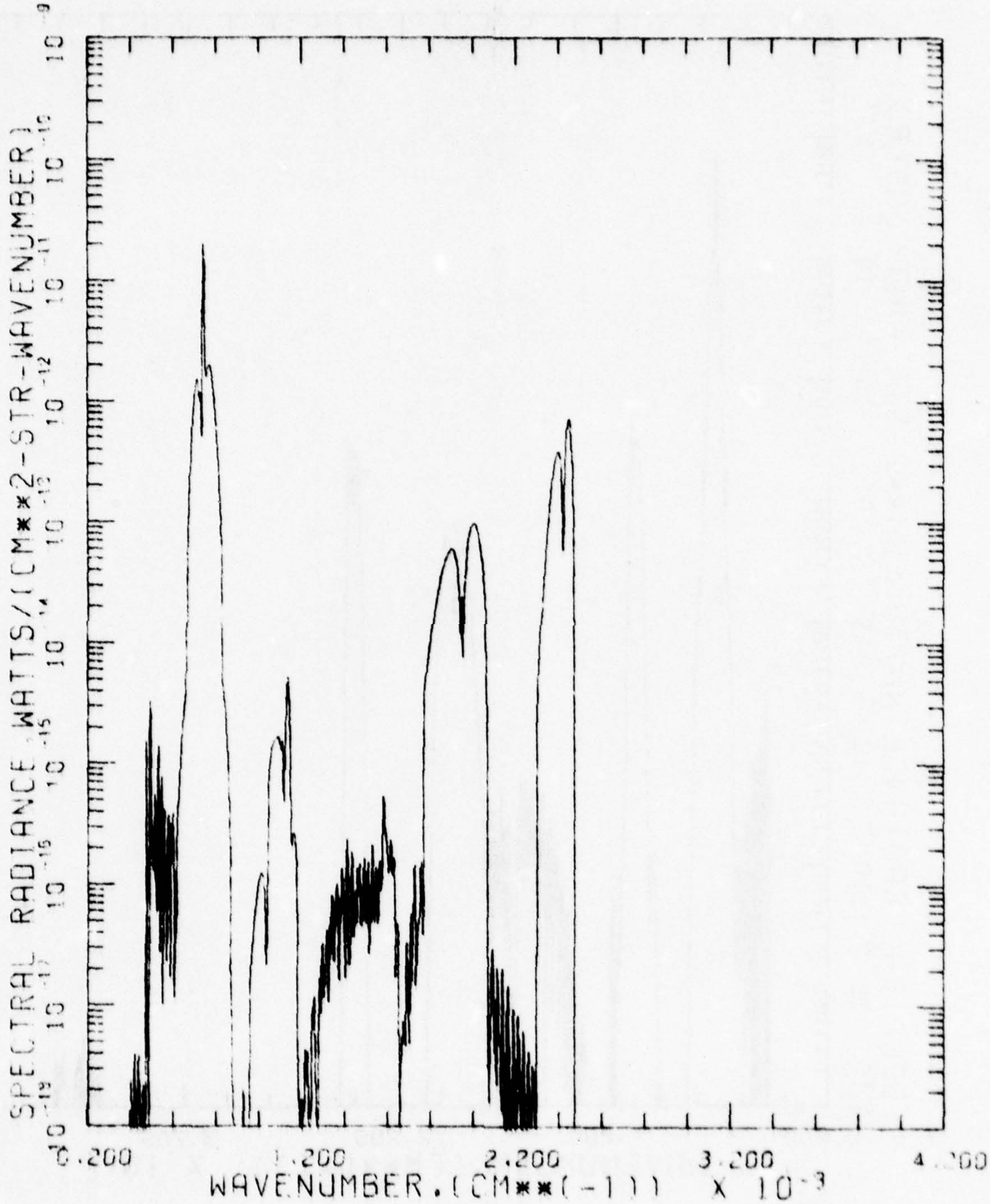


Fig. 34 Night Vertical Viewing Radiance at 150 Km Altitude.

Program FLASH

The program uses the backward Monte Carlo method for studying multiple scattering and absorption in spherical-shell atmosphere. In region of the upper atmosphere where the present study is focused, the background photons scattered by either the Rayleigh particles or the aerosols would reach the sensor most likely by going through only a single deflection. A simple calculation can show that a probability of multiple scattering is quite small and in fact the FLASH confirms this notion. However, at present, our calculations of the scattered radiance level are all carried out by the FLASH.

After considerable difficulty running the FLASH during the early stage of our study, even with the assistance available from Blättner, we eventually have succeeded to decipher a general structure of the FLASH. We believe that the program execution devised by us is proper. Currently the program runs with the input data specified by

(1) the spectral region in $cm^{-1}$;

(2) the sensor altitude in km;

(3) the sensor azimuth angle; and

(4) the solar angles (a set of 7 values). (See Appendix A for structure of Job Submit Deck.)

The sensor zenith angles are automatically set for values of 17 tangent heights ranging from 50 km to 160 km with 10 km increment. The input data to the FLASH are first arranged and streamlined by running a small program called PRFLASH. The source listing of PRFLASH and other pertinent informations are also given in Appendix A.

Figs. 35 through 37 show the spectral dependence of the scattered radiance level as a function of the tangent heights. The figure for 150 km tangent height indicates the Rayleigh scattering of $1/\lambda^4$ dependency, reflecting the assumed atmospheric model by the FLASH.

The FLASH computes the scattered radiance level as a function of the solar angle $\theta$, the sensor's azimuth angle $\phi$ and zenith angle $\rho$. Once the single scattering dominates other processes, the radiance level is essentially controlled by the scattering angle $\Theta$ only. The curves shown in Figs. 38 through 40 are plotted against the scattering angle $\Theta$, even though the original data are computed with various sets of $(\theta, \phi, \rho)$. See Fig. 41 for these angles. These curves strongly indicate that the radiance levels are indeed a function of the scattering angle $\Theta$ only, and that other processes considered in the FLASH are negligible.

The computed results by the FLASH and by the DEGGES are superimposed in Figs. 42 through 45. The curves by the FLASH are for the scattering angle close to $90^{\circ}$, the worst expected case in the computed results. The curve for the limb viewing at 60 km tangent height shows that the scattering and the emission radiance level are about equal. Toward higher tangent height, the scattering radiation falls off more rapidly than the emission radiance.

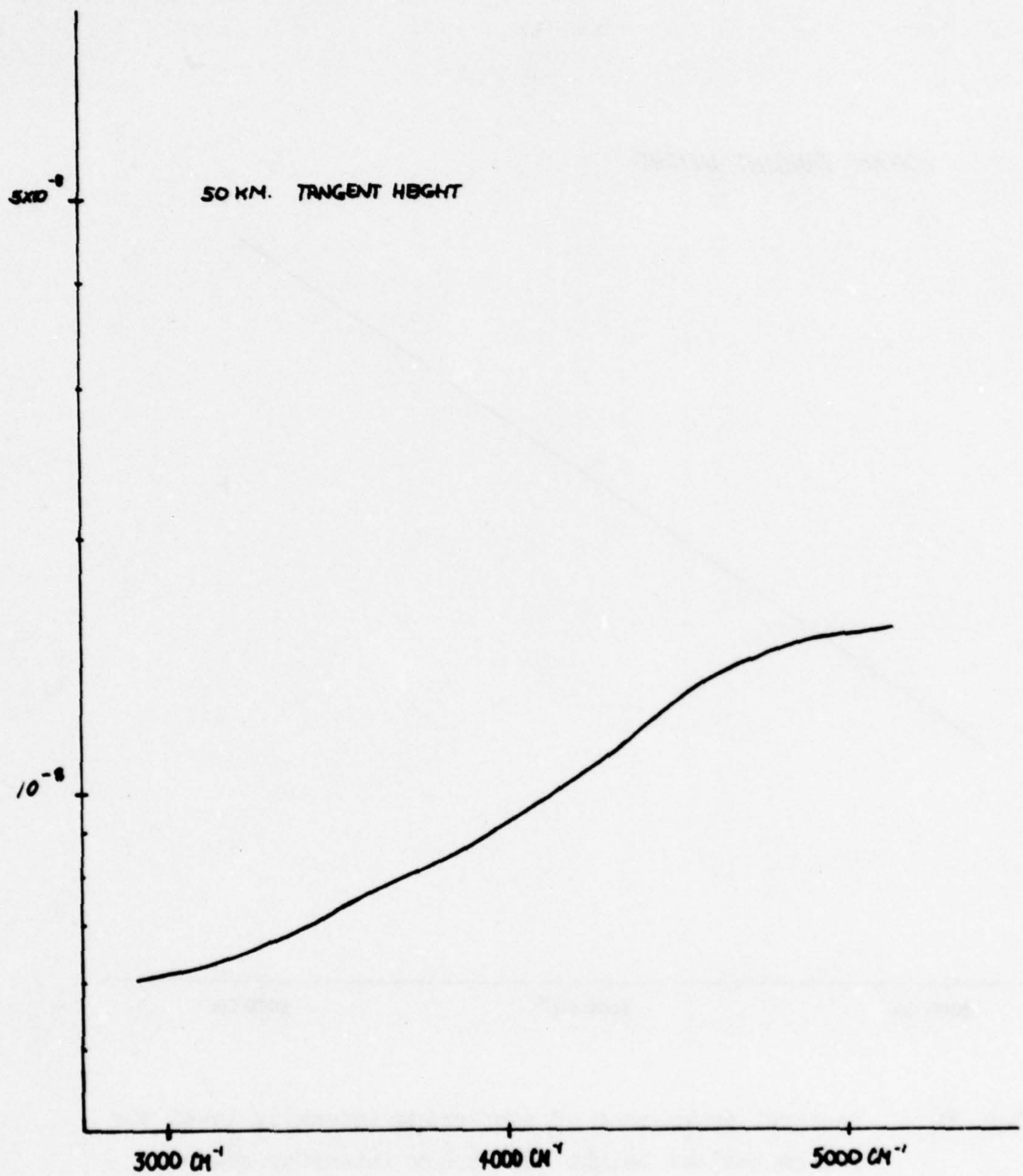


Fig. 35 Spectral dependence of scattering intensity level for 50 km tangent height (arbitrary intensity scale)

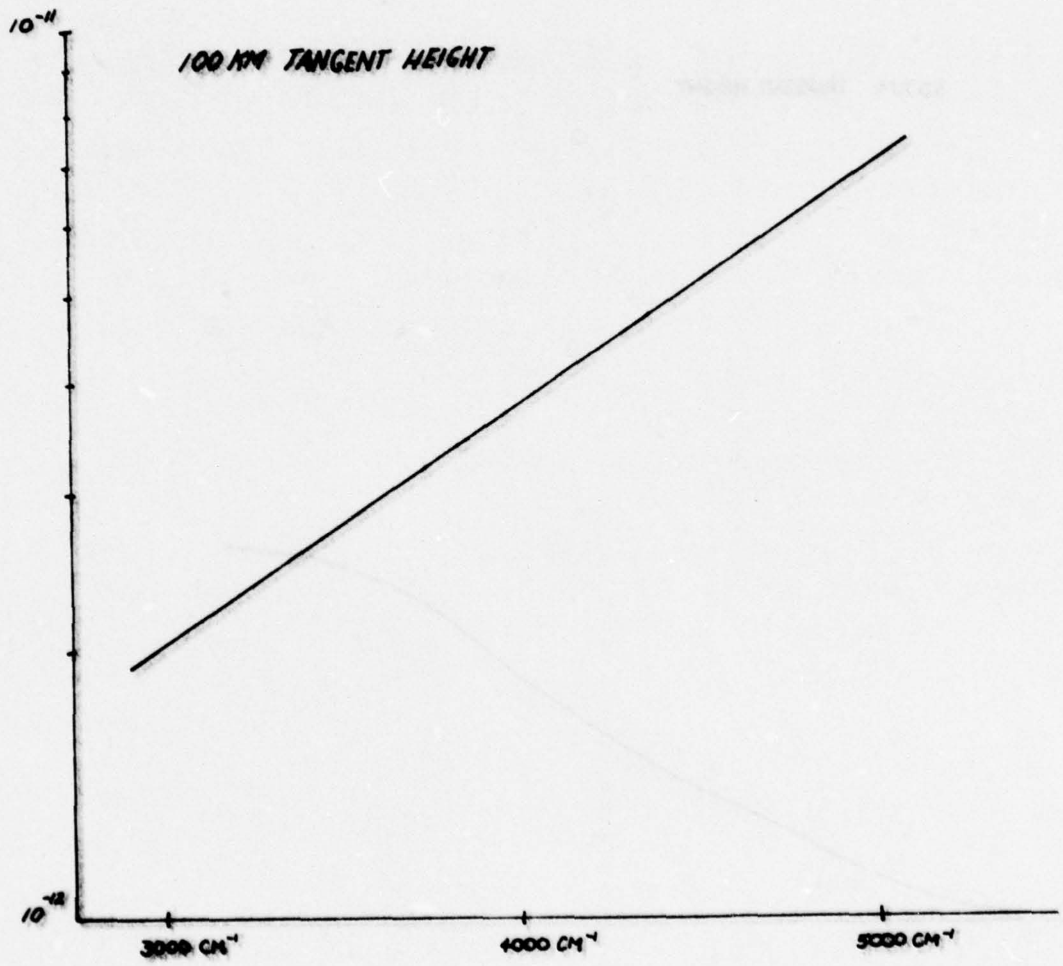


Fig. 36 Spectral dependence of scattering intensity level for 100 km tangent height (arbitrary intensity scale)

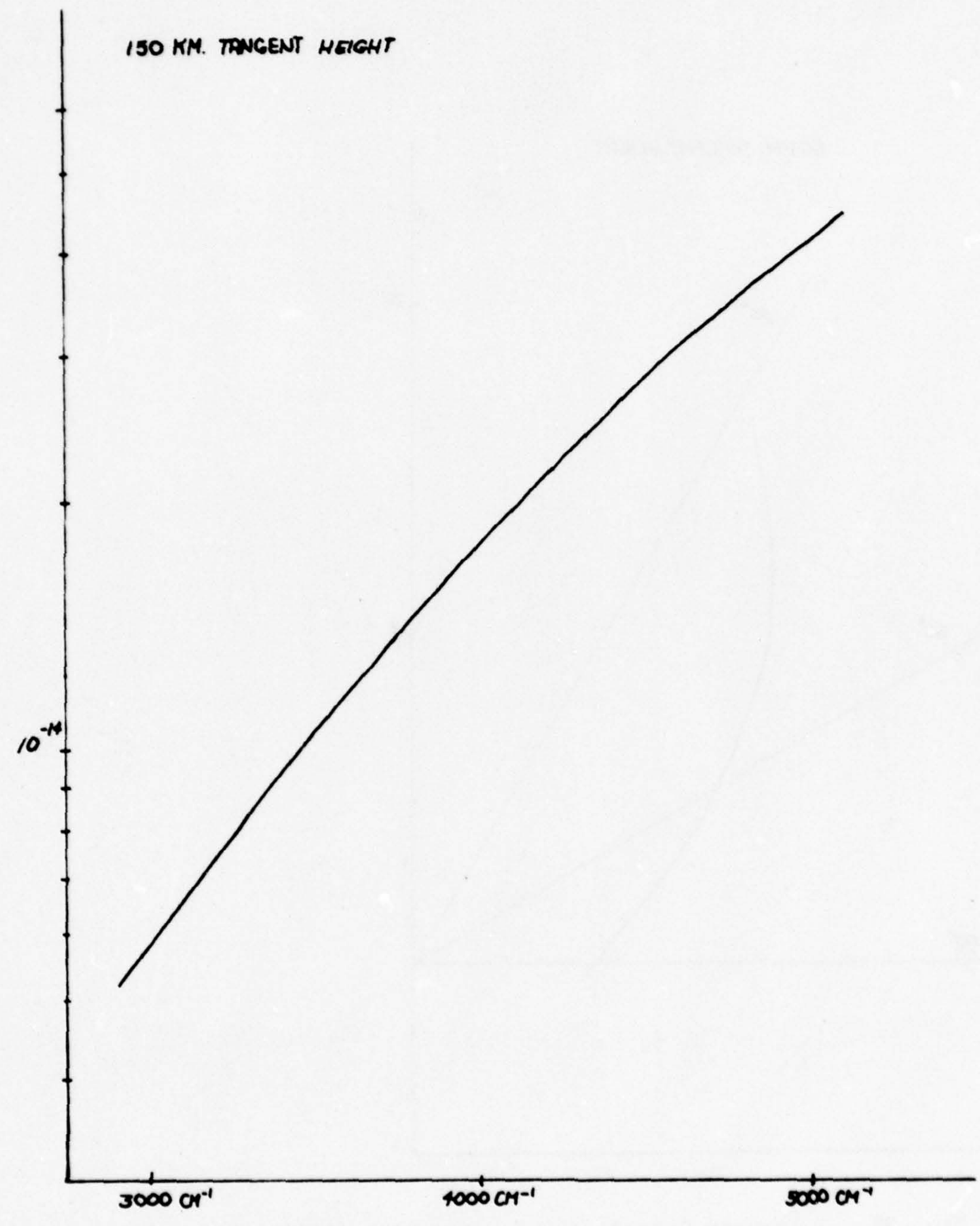


Fig. 37 Spectral dependence of scattering intensity level for 150 km tangent height (arbitrary intensity scale)

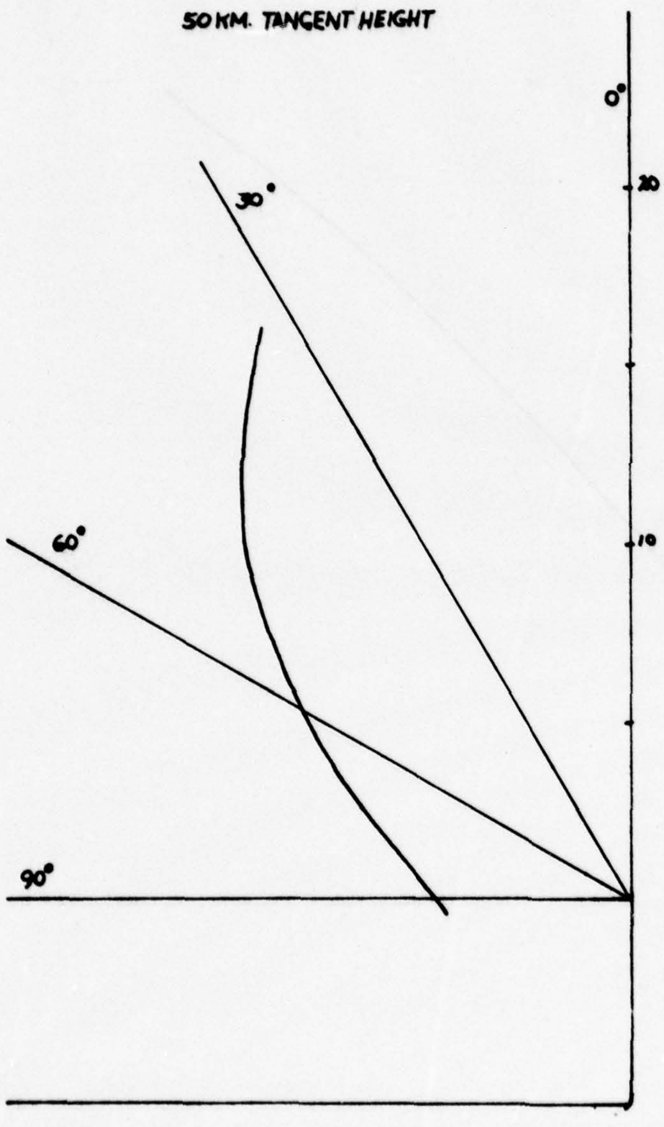


Fig. 38 Angular dependence of scattering intensity level for 50 km tangent height (arbitrary intensity scale)

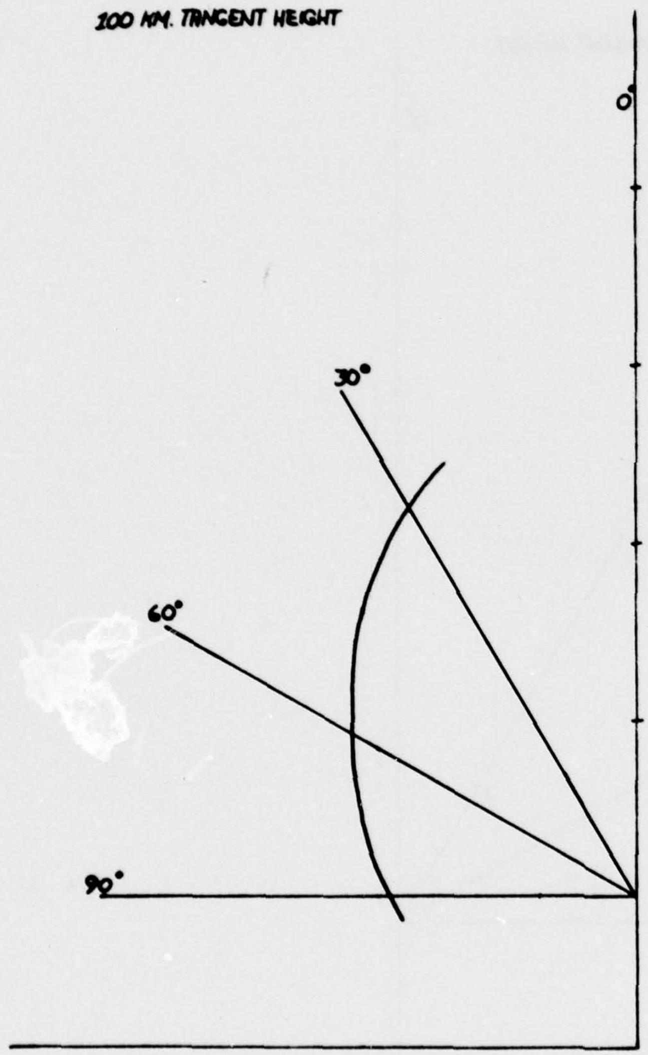


Fig. 39 Angular dependence of scattering intensity level for 100 km tangent height (arbitrary intensity scale)

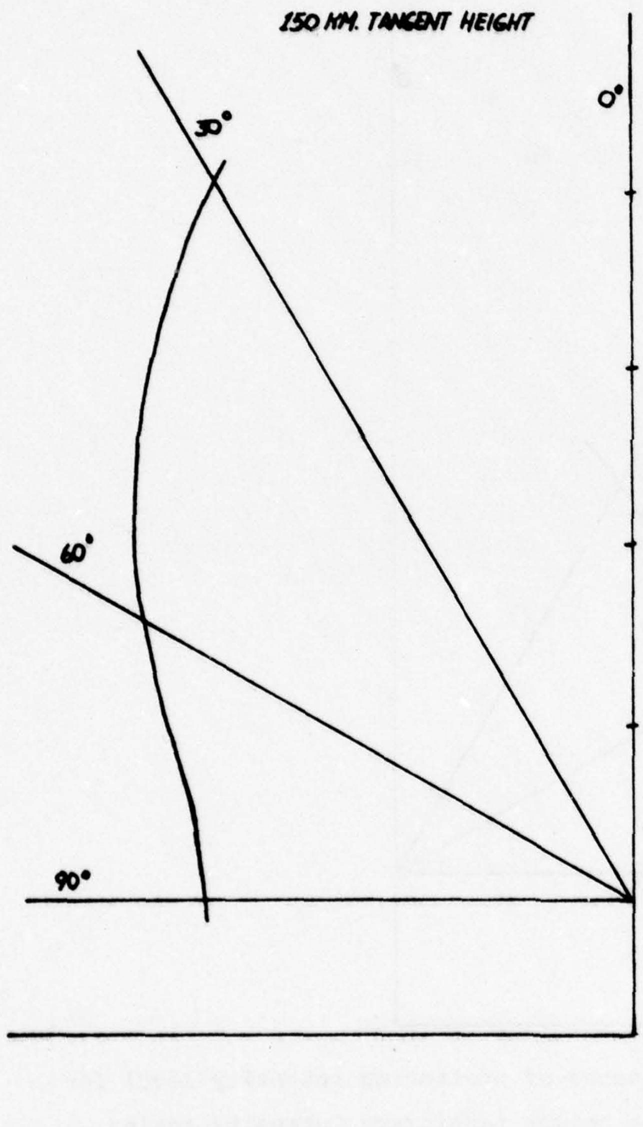


Fig. 40 Angular dependence of scattering intensity level for 150 km tangent height (arbitrary intensity scale)

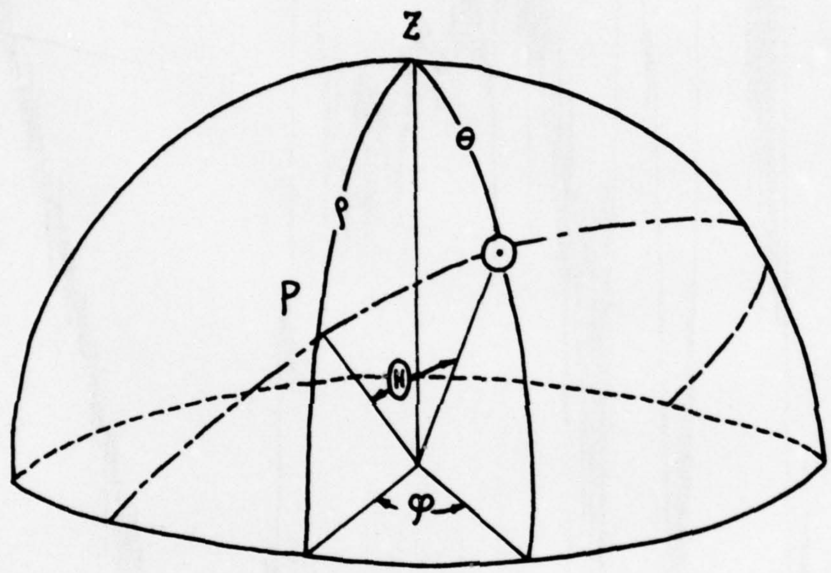


Fig. 41 Definition of 4 angles, θ, ϕ, ρ and H

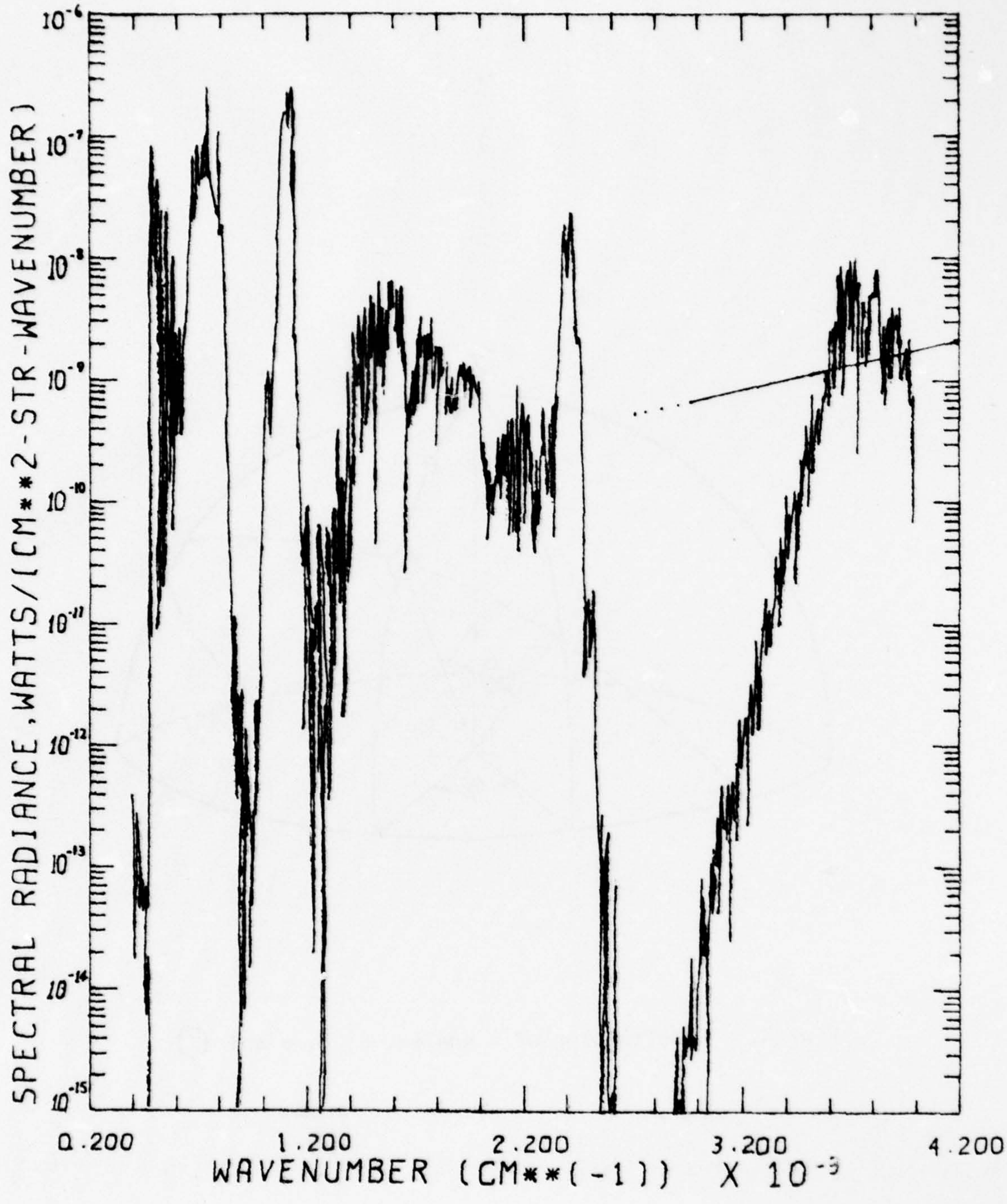


Fig. 42 Day Limb Viewing Radiance at 60 km Tangent Height

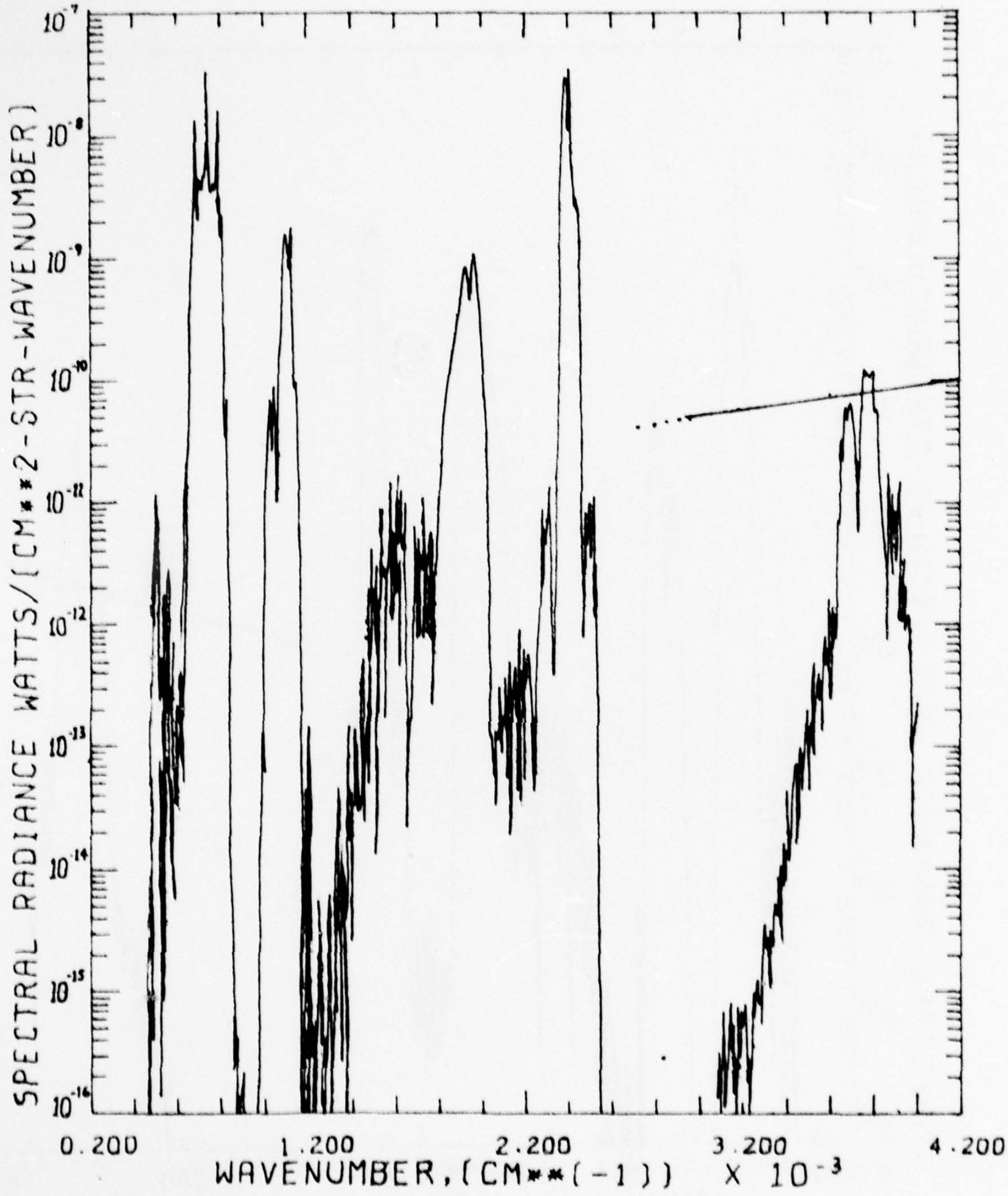


Fig. 43 Day Limb Viewing Radiance at 80 km Tangent Height

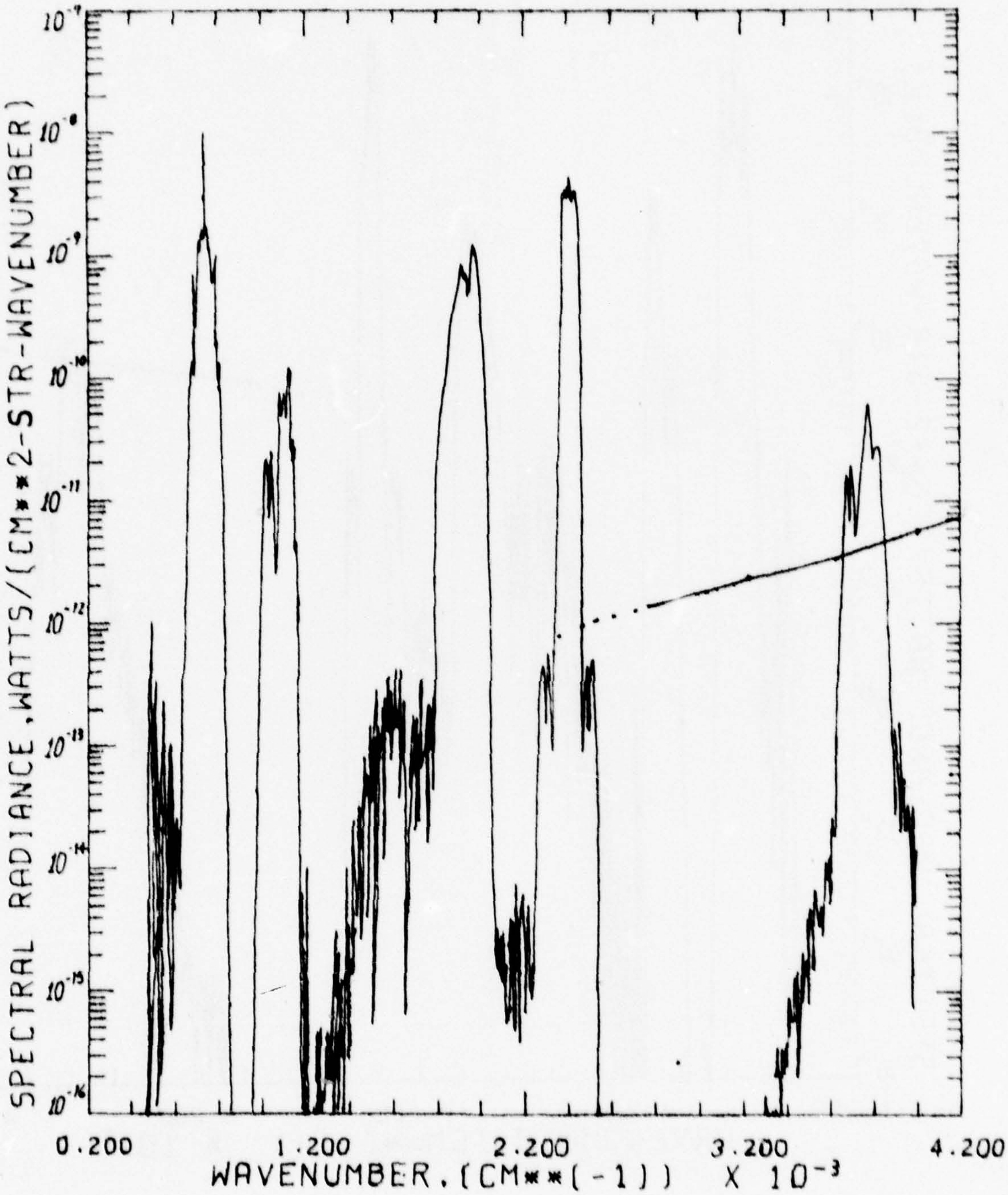


Fig. 44 Day Limb Viewing at 100 km Tangent Height

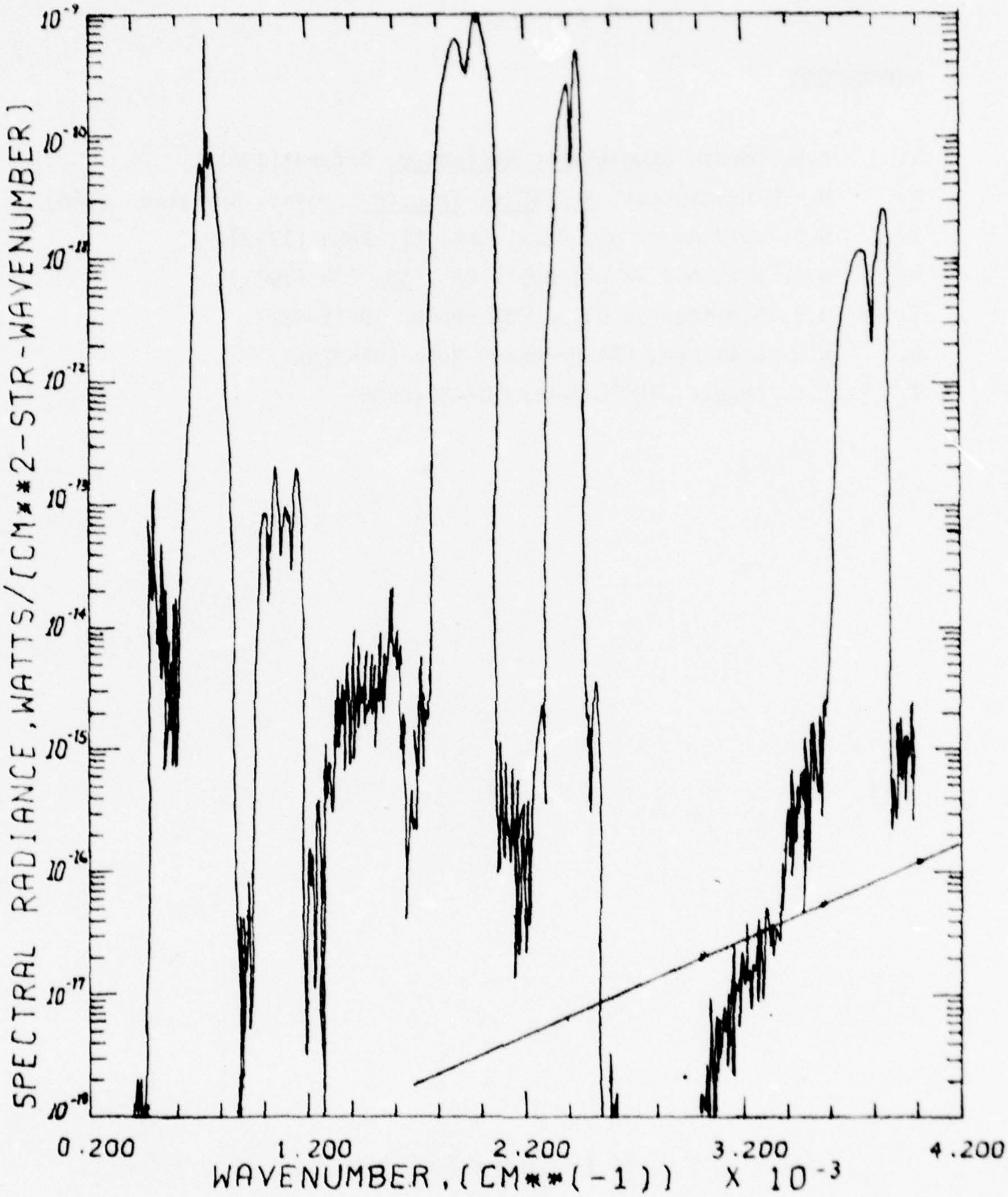


Fig. 45 Day Limb Viewing Radiance at 150 km Tangent Height

REFERENCES


1. R.M. Goody, Atmospheric Radiation, Oxford (1964).
2. S. Chandrasekhar, Radiative Transfer, Dover, New York (1960).
3. D.G. Collins *et al*, Appl. Opt. 11, 2684 (1972).
4. W.G. Blättner *et al*, Appl. Opt. 13, 534 (1974).
5. W.G. Blättner *et al*, AFCRL Report TR-75-0317.
6. W.G. Blättner, RRA Research Note RRA-N7512.
7. T.C. Degges, AFCRL Report TR-74-0606.

Appendix A

1. Source Listing of PRFLASH and CRW

```
      PROGRAM PRFLASH(TAPE1,TAPE5=200B,TAPE7=200B,TAPE8=200B,TAPE9,
     1TAPE10=200B)
      DIMENSION WREF(128)
      DIMENSION A(128),X(16),AA(16)
      DIMENSION ATHETA(16)
  101 FORMAT(8F10.3)
  102 FORMAT(F7.2)
  103 FORMAT(F10.4,I10)
  104 FORMAT(I5,F8.0)
  105 FORMAT(8I10)
      DO 25 I=1,128
   25 WREF(I)=0.
      REWIND 7
      REWIND 8
      REWIND 5
      REWIND 9
      REWIND 1
      READ(7,101) W,AL,AZ
      READ(7,101)(ATHETA(I),I=1,7)
      WX=W
   27 CONTINUE
      READ(10,104) N,WREF(N)
      IF(N.NE.70) GO TO 27
      DO 28 I=39,70
      L=I
      IF(W.LE.WREF(L)) GO TO 29
   28 CONTINUE
   29 LA=L-1
      DO 30 I=3,35
      L=I
      IF(W.LE.WREF(L)) GO TO 31
   30 CONTINUE
   31 LB=L-1
      LC=0
      J=9
      DO 10 I=1,9
      X(J)=10000./WX
      WX=WX+20.
      J=J-1
   10 CONTINUE
      XX=0.5*(X(1)+X(9))
      WA=W-100.
      WB=WX+100.
      CALL CRW(5,1)
      CALL CRW(2,0)
      WRITE(5,101)(X(I),I=1,6)
      WRITE(5,101)(X(I),I=7,9)
      CALL CRW(147,1)
      WRITE(5,102)XX
      CALL CRW(1,0)
      CALL CRW(27,1)
      CALL CRW(1,0)
      WRITE(5,105) LC,LA
      CALL CRW(4,1)
      CALL CRW(1,0)
      WRITE(5,105) LC,LB
      CALL CRW(10,1)
```

```
      WRITE(5,101)(ATHETA(I),I=1,6)
      WRITE(5,101) ATHETA(7)
      CALL CRW(3,0)
      IC=14
      WRITE(5,103) AL ,IC
      CALL CRW(2,1)
      Y=AL+6357.
      Z=20.+6357.
      DO 20 J=1,IC
      AXX=Z/Y
      AA(J)=180.-(ASIN(AXX)*180./3.1415926)
      Z=Z+10.
   20 CONTINUE
      DO 21 J=1,14
      AAA=AA(J)-.1
      AAB=AA(J)+.1
      AZB=AZ+.1
      AZA=AZ-.1
      WRITE(5,101) AAA,AAB
      WRITE(5,101) AZA,AZB
   21 CONTINUE
      CALL CRW(28,0)
      CALL CRW(7,1)
      REWIND 9
      IF(WB.GE.12000.) GO TO 60
   40 CONTINUE
      READ(9)(A(I),I=1,99)
      IF(A(1).GE.WB) GO TO 50
      IF((A(1).GE.WA).AND.(A(1).LT.WB))
     1 WRITE(1) (A(I),I=1,99)
      GO TO 40
   60 CONTINUE
      DO 70 I=1,99
      A(I)=0.
   70 CONTINUE
      A(1)=WA
   71 CONTINUE
      WRITE(1)(A(I),I=1,99)
      A(1)=A(1)+5.
      IF(A(1).LE.WB) GO TO 71
      CONTINUE
   50 CONTINUE
      REWIND 1
      CALL EXIT
      STOP
      END
```

```
      SUBROUTINE CRW(K,L)
      DIMENSION A(16)
  100 FORMAT(8A10)
      DO 10 J=1,K
      READ(8,100)(A(I),I=1,8)
      IF(L.NE.0) WRITE(5,100)(A(I),I=1,8)
   10 CONTINUE
      RETURN
      END
```

2. Job Submit Deck.

```
JOBCARD
ACCOUNT#        T40, CM12000.
ATTACH,FLASH.
GET,FLASHDE.
GET,FLASHB2.
GET,TP3DATA.
COPYCR,TP3DATA,TAPE10.
REWIND,TAPE10.
GET,FLASHB.
SKIPF,FLASH,2.
COPYBF,FLASH,TAPE9.
PACK,TAPE9.
COPYCR,INPUT,TAPE7.
COPYCR,FLASHDE,TAPE8.
REWIND,TAPE7,TAPE8,TAPE9.
MAP,PART.
FLASHB2.                          ;OBJECT PROGRAM OF PRFLASH
COPYBF,FLASH,TAPE3.
PACK,TAPE3.
REWIND,TAPE1,TAPE3,TAPE5.
FLASHB.                           ;OBJECT PROGRAM OF FLASH
REWIND,TAPE4.
COPYCR,TAPE4,OUTPUT.
REWIND,TAPE4.
COPYCR,TAPE4,FLASHOT.
REWIND,TAPE6.
COPYCR,TAPE6,OUTPUT.
EXIT.
REWIND,TAPE6.
COPYCR,TAPE6,OUTPUT.
 7/8/9
   5000.        200.        67.
     24.         34.        44.        54.        64.        74.        84.
```

3. Tape 8

```
      1
PROBLEM 200.
      1        70        10         0         1         1
   6.35700E 03
      9       20.       -1.
  2.39521   2.38329   2.37248   2.36128   2.35018   2.33918
  2.32829   2.31750   2.30681
.11111111 .11111111 .11111111 .11111111 .11111111 .11111111 .11111111
.11111111 .11111111 .11111111
    288.2 1.013E+03       0.0
    286.5 9.836E+02      0.25
    284.9 9.546E+02       0.5
    283.3 9.264E+02      0.75
    281.7 8.988E+02       1.0
    278.4 8.456E+02       1.5
    275.2 7.950E+02       2.0
    268.7 7.012E+02       3.0
    262.2 6.166E+02       4.0
    255.7 5.405E+02       5.0
    249.2 4.722E+02       6.0
    242.7 4.111E+02       7.0
    236.2 3.565E+02       8.0
    229.7 3.080E+02       9.0
    223.3 2.650E+02      10.0
    216.8 2.227E+02      11.0
    216.7 1.940E+02      12.0
    216.7 1.658E+02      13.0
    216.7 1.417E+02      14.0
    216.7 1.211E+02      15.0
    216.7 1.035E+02      16.0
    216.7 8.850E+01      17.0
    216.7 7.565E+01      18.0
    216.7 6.467E+01      19.0
    216.7 5.529E+01      20.0
    216.7 4.729E+01      21.0
    217.6 4.048E+01      22.0
    218.6 3.467E+01      23.0
    219.6 2.972E+01      24.0
    220.6 2.549E+01      25.0
    221.6 2.188E+01      26.0
    222.5 1.880E+01      27.0
    223.5 1.616E+01      28.0
    224.5 1.390E+01      29.0
    226.5 1.197E+01      30.0
    228.5 8.891E+00      32.0
    233.7 6.631E+00      34.0
    239.3 4.985E+00      36.0
    244.8 3.771E+00      38.0
```

| | | |
|---|---|---|
| 250.4 | 2.871E+00 | 40.0 |
| 255.9 | 2.200E+00 | 42.0 |
| 261.4 | 1.695E+00 | 44.0 |
| 266.9 | 1.313E+00 | 46.0 |
| 270.7 | 1.023E+00 | 48.0 |
| 270.7 | 7.978E-01 | 50.0 |
| 265.6 | 4.275E-01 | 55.0 |
| 255.8 | 2.246E-01 | 60.0 |
| 239.3 | 1.145E-02 | 65.0 |
| 219.7 | 5.521E-02 | 70.0 |
| 201.3 | 2.400E-02 | 75.0 |
| 186.0 | 9.745E-03 | 80.0 |
| 186.0 | 3.986E-03 | 85.0 |
| 186.0 | 1.633E-03 | 90.0 |
| 199.5 | 6.907E-04 | 95.0 |
| 213.0 | 3.095E-04 | 100.0 |
| 263.0 | 7.690E-05 | 110.0 |
| 380.7 | 2.733E-05 | 120.0 |
| 524.3 | 1.315E-05 | 130.0 |
| 644.8 | 7.501E-06 | 140.0 |
| 750.6 | 4.696E-06 | 150.0 |
| 848.9 | 3.126E-06 | 160.0 |
| 942.6 | 2.176E-06 | 170.0 |
| 1032.3 | 1.569E-06 | 180.0 |
| 1117.6 | 1.162E-06 | 190.0 |
| 1198.4 | 8.806E-07 | 200.0 |
| 1271.8 | 6.794E-07 | 210.0 |
| 1341.8 | 5.322E-07 | 220.0 |
| 1408.0 | 4.222E-07 | 230.0 |
| 1468.4 | 3.386E-07 | 240.0 |
| 1524.7 | 2.741E-07 | 250.0 |

| | | | | | | | |
|---|---|---|---|---|---|---|---|
| 5.9E-00 | 7.641E 15 | 5.4E-05 | 1.274E 13 | 1.910E 12 | 3.567E 13 | 5.336E 18 | 0.0 |
| 5.45E-00 | 7.460E 15 | 5.4E-05 | 1.244E 13 | 1.865E 12 | 3.481E 13 | 5.209E 18 | 0.25 |
| 5.0E-00 | 7.281E 15 | 5.4E-05 | 1.214E 13 | 1.820E 12 | 3.398E 13 | 5.085E 18 | .5 |
| 4.55E-00 | 7.106E 15 | 5.4E-05 | 1.185E 13 | 1.777E 12 | 3.316E 13 | 4.962E 18 | 0.75 |
| 4.2E-00 | 6.935E 15 | 5.4E-05 | 1.156E 13 | 1.734E 12 | 3.236E 13 | 4.842E 18 | 1.0 |
| 3.55E-00 | 6.600E 15 | 5.4E-05 | 1.100E 13 | 1.650E 12 | 3.080E 13 | 4.609E 18 | 1.5 |
| 2.9E-00 | 6.279E 15 | 5.4E-05 | 1.046E 13 | 1.570E 12 | 2.930E 13 | 4.384E 18 | 2.0 |
| 1.8E-00 | 5.672E 15 | 5.0E-05 | 9.453E 12 | 1.418E 12 | 2.647E 13 | 3.961E 18 | 3.0 |
| 1.1E-00 | 5.111E 15 | 4.6E-05 | 8.519E 12 | 1.278E 12 | 2.385E 13 | 3.569E 18 | 4.0 |
| 6.4E-01 | 4.594E 15 | 4.6E-05 | 7.657E 12 | 1.148E 12 | 2.144E 13 | 3.208E 18 | 5.0 |
| 3.8E-01 | 4.118E 15 | 4.5E-05 | 6.863E 12 | 1.029E 12 | 1.922E 13 | 2.875E 18 | 6.0 |
| 2.1E-01 | 3.680E 15 | 4.9E-05 | 6.134E 12 | 9.201E 11 | 1.718E 13 | 2.570E 18 | 7.0 |
| 1.2E-01 | 3.280E 15 | 5.2E-05 | 5.467E 12 | 8.120E 11 | 1.531E 13 | 2.290E 18 | 8.0 |
| 4.6E-02 | 2.913E 15 | 7.1E-05 | 4.856E 12 | 7.284E 11 | 1.360E 13 | 2.034E 18 | 9.0 |
| 1.8E-02 | 2.579E 15 | 9.0E-05 | 4.299E 12 | 6.449E 11 | 1.204E 13 | 1.801E 18 | 10.0 |
| 8.2E-03 | 2.276E 15 | 1.3E-04 | 3.793E 12 | 5.689E 11 | 1.062E 13 | 1.589E 18 | 11.0 |
| 3.7E-03 | 1.946E 15 | 1.6E-04 | 3.243E 12 | 4.865E 11 | 9.081E 12 | 1.359E 18 | 12.0 |
| 1.8E-03 | 1.663E 15 | 1.7E-04 | 2.772E 12 | 4.157E 11 | 7.761E 12 | 1.161E 18 | 13.0 |
| 8.4E-04 | 1.421E 15 | 1.9E-04 | 2.369E 12 | 3.553E 11 | 6.633E 12 | 9.925E 17 | 14.0 |
| 7.2E-04 | 1.215E 15 | 2.1E-04 | 2.025E 12 | 3.037E 11 | 5.669E 12 | 8.483E 17 | 15.0 |
| 6.1E-04 | 1.038E 15 | 2.4E-04 | 1.731E 12 | 2.596E 11 | 4.846E 12 | 7.251E 17 | 16.0 |
| 5.2E-04 | 8.877E 14 | 2.8E-04 | 1.479E 12 | 2.219E 11 | 4.142E 12 | 6.199E 17 | 17.0 |
| 4.4E-04 | 7.588E 14 | 3.2E-04 | 1.265E 12 | 1.897E 11 | 3.541E 12 | 5.299E 17 | 18.0 |
| 4.4E-04 | 6.487E 14 | 3.5E-04 | 1.081E 12 | 1.622E 11 | 3.027E 12 | 4.530E 17 | 19.0 |
| 4.4E-04 | 5.546E 14 | 3.8E-04 | 9.244E 11 | 1.387E 11 | 2.588E 12 | 3.873E 17 | 20.0 |
| 4.8E-04 | 4.723E 14 | 3.8E-04 | 7.872E 11 | 1.181E 11 | 2.204E 12 | 3.298E 17 | 21.0 |
| 5.2E-04 | 4.024E 14 | 3.9E-04 | 6.707E 11 | 1.006E 11 | 1.878E 12 | 2.810E 17 | 22.0 |
| 5.7E-04 | 3.431E 14 | 3.8E-04 | 5.719E 11 | 8.578E 10 | 1.601E 12 | 2.396E 17 | 23.0 |
| 6.1E-04 | 2.928E 14 | 3.6E-04 | 4.880E 11 | 7.320E 10 | 1.366E 12 | 2.045E 17 | 24.0 |
| 6.6E-04 | 2.500E 14 | 3.4E-04 | 4.167E 11 | 6.251E 10 | 1.167E 12 | 1.746E 17 | 25.0 |
| 6.6E-04 | 2.137E 14 | 3.1E-04 | 3.562E 11 | 5.342E 10 | 9.972E 11 | 1.492E 17 | 26.0 |
| 6.0E-04 | 1.828E 14 | 2.9E-04 | 3.047E 11 | 4.569E 10 | 8.529E 11 | 1.276E 17 | 27.0 |
| 5.2E-04 | 1.564E 14 | 2.6E-04 | 2.607E 11 | 3.911E 10 | 7.300E 11 | 1.092E 17 | 28.0 |
| 4.4E-04 | 1.340E 14 | 2.3E-04 | 2.234E 11 | 3.350E 10 | 6.252E 11 | 9.356E 16 | 29.0 |
| 3.6E-04 | 1.148E 14 | 2.0E-04 | 1.914E 11 | 2.871E 10 | 5.359E 11 | 8.019E 16 | 30.0 |

```
2.0E-04 8.456E 13    1.6E-04 1.409E 11 2.114E 10 3.946E 11 5.904E 16       32.0
1.4E-04 6.168E 13    1.3E-04 1.028E 11 1.542E 10 2.878E 11 4.307E 16       34.0
9.1E-05 4.527E 13    9.5E-05 7.546E 10 1.132E 10 2.113E 11 3.161E 16       36.0
6.0E-05 3.348E 13    5.9E-05 5.580E 10 8.369E 09 1.562E 11 2.338E 16       38.0
4.3E-05 2.492E 13    4.9E-05 4.154E 10 6.231E 09 1.163E 11 1.740E 16       40.0
3.0E-05 1.868E 13    3.5E-05 3.114E 10 4.670E 09 8.717E 10 1.305E 16       42.0
2.1E-05 1.409E 13    2.1E-05 2.348E 10 3.523E 09 6.576E 10 9.839E 15       44.0
1.4E-05 1.069E 13    1.4E-05 1.782E 10 2.673E 09 4.990E 10 7.467E 15       46.0
1.0E-05 8.213E 12    9.0E-06 1.369E 10 2.053E 09 3.833E 10 5.735E 15       48.0
6.3E-06 6.406E 12    4.0E-06 1.068E 10 1.601E 09 2.989E 10 4.473E 15       50.0
2.5E-06 3.498E 12    2.0E-06 5.832E 09 8.745E 08 1.632E 10 2.443E 15       55.0
1.2E-06 1.908E 12    9.6E-07 3.181E 09 4.771E 08 8.905E 09 1.333E 15       60.0
4.7E-07 1.040E 12    4.2E-07 1.734E 09 2.599E 08 4.851E 09 7.139E 14       65.0
2.0E-07 5.460E 11    1.6E-07 9.101E 08 1.365E 08 2.548E 09 3.586E 14       70.0
9.0E-08 2.704E 11    4.0E-08 5.100E 08 6.760E 07 1.262E 09 1.737E 14       75.0
1.5E-08 4.962E 10    2.0E-08 9.300E 07 1.241E 07 5.820E 08 3.251E 13       85.0
3.9E-08 1.247E 11    1.3E-08 1.100E 08 3.118E 07 2.316E 08 7.950E 13       80.0
5.4E-09 1.977E 10    5.6E-09 9.300E 07 4.943E 06 9.227E 07 1.332E 13       90.0
1.8E-09 7.560E 09    8.0E-10 1.000E 08 1.890E 06 3.528E 07 5.190E 12       95.0
7.5E-10 3.111E 09    9.6E-11 1.100E 08 7.778E 05 1.452E 07 1.994E 12      100.0
1.3E-10 5.236E 08    2.7E-12 9.000E 07                     3.492E 11      110.0
3.9E-11 8.817E 07    1.7E-13 7.000E 07                     7.495E 10      120.0
1.4E-11 1.485E 07    8.0E-16 5.200E 07                     2.343E 10      130.0
6.6E-12 2.500E 06    7.2E-18 3.900E 07                     9.795E  9      140.0
3.3E-12 4.210E 05    5.3E-20 3.000E 07                     4.777E  9      150.0
1.5E-12 7.088E 04    4.4E-22 2.300E 07                     2.559E  9      160.0
7.5E-13 1.194E 04    2.4E-26 1.800E 07                     1.467E  9      170.0
3.6E-13 2.010E 03    2.0E-28 1.300E 07                     8.825E  8      180.0
1.6E-13 3.384E 02    1.3E-30 9.800E 06                     5.528E  8      190.0
7.8E-14 5.679E 01            7.400E 06                     3.572E  8      200.0
3.7E-14 9.596E 00            5.500E 06                     2.372E  8      210.0
1.8E-14 1.616E 00            4.300E 06                     1.607E  8      220.0
8.7E-15 2.721E-01            3.300E 06                     1.107E  7      230.0
4.2E-15 4.581E-02            2.700E 06                     7.748E  7      240.0
2.0E-15 7.714E-03            1.900E 06                     5.491E 07      250.0
      2
     0.
     0.         0.          0.          1.          0.        -1.
    10.      1000.
 2.54710E 19    0.02950E 00    1.01330E 03    2.88150E 02
2.35
    0.167340          0.044449
    0.13971           0.20020
1.989E 19 1.942E 19 1.895E 19 1.850E 19 1.805E 19 1.718E 19 1.634E 19 1.476E 19
1.330E 19 1.196E 19 1.072E 19 9.580E 18 8.537E 18 7.584E 18 6.714E 18 5.923E 18
5.065E 18 4.329E 18 3.700E 18 3.162E 18 2.703E 18 2.311E 18 1.975E 18 1.689E 18
1.444E 18 1.229E 18 1.047E 18 8.931E 17 7.621E 17 6.508E 17 5.562E 17 4.757E 17
4.072E 17 3.487E 17 2.989E 17 2.201E 17 1.605E 17 1.178E 17 8.714E 16 6.488E 16
4.863E 16 3.668E 16 2.783E 16 2.138E 16 1.667E 16 9.105E 15 5.103E 15 2.661E 15
1.337E 15 6.474E 14 2.963E 14 1.212E 14 4.965E 13 1.947E 13 8.178E 12 1.620E 12
4.008E 11 1.396E 11 6.357E 10 3.336E 10 1.907E 10 1.160E 10 7.368E  9 4.857E  9
3.293E  9 2.291E  9 1.622E  9 1.167E  9 8.510E  8 6.281E  8
   1970
    6.8        5.4        4.7        4.0        3.3        2.8
    2.28       1.5        1.0        0.72       0.57       0.6
    0.67       0.72       0.82       0.92       0.95       1.0
    1.15       1.32       1.45       1.28       1.25       1.4
    1.23       1.12       0.95       0.77       0.75       0.7
    0.65       0.60       0.45       0.35       0.25       0.08
    0.05       0.05       0.05       0.05       0.05       0.05
    0.05       0.05       0.05       0.05       0.05       0.05
    0.05       0.05       0.05       0.05       0.05       0.05
    0.05       0.0        0.0        0.0        0.0        0.0
    0.0        0.0        0.0        0.0        0.0        0.0
    0.0        0.0        0.0        0.0
```

```
TROPOSPERIC AEROSOLS - HAZE C.
         2         1         0         0         0         1         3
       100       100        1.
         0        54
STRATOSPHERIC AEROSOLS - 'FRIEND PARTICLES'.
         2         2         0         0         1         1         3
  0.0295
       100       100        1.
         0        17
ALBEDO = 0.2.
         3         1         0         0
   0.20000E 00    0.00000E 00    1.00000E 00
TROPOPAUSE AT 10KM ALTITUDE.
         4         2         1
      -10.       10.        1.         1
       10.     1000.        1.         2
0.
RECEIVER VIEW ANGLES FOR RAD = 200 KM ALTITUDE.
         5         7
       24.       44.       54.       64.       84.       94
       94.
  199.9999        14
         1         1         1         1         1         1         1
         1         1         1         1         1         1         1
    103.44    103.44
      67.0      67.0
    103.05    103.05
      67.0      67.0
    102.66    102.66
      67.0      67.0
    102.27    102.27
      67.0      67.0
    101.89    101.89
      67.0      67.0
    101.50    101.50
      67.0      67.0
    101.11    101.11
      67.0      67.0
    100.73    100.73
      67.0      67.0
    100.34    100.34
      67.0      67.0
     99.57     99.57
      67.0      67.0
     98.79     98.79
      67.0      67.0
     98.02     98.02
      67.0      67.0
     97.25     97.25
      67.0      67.0
     96.48     96.48
      67.0      67.0
CONSTANTS.
         6   2002350
       112        20         9         1         1
0.100E-03 0.100E-03 0.100E-01 0.100E-07 0.200E 02
         1         0         1        -1        -1
   0.60200E-02
   0.             0.             1.             1.
```

4. Tape 10

| | | | |
|---|---|---|---|
| 3 | 2083. | 39 | 2083. |
| 4 | 2326. | 40 | 2326. |
| 5 | 2632. | 41 | 2632. |
| 6 | 3125. | 42 | 3125. |
| 7 | 3226. | 43 | 3226. |
| 8 | 3333. | 44 | 3333. |
| 9 | 3448. | 45 | 3448. |
| 10 | 3509. | 46 | 3509. |
| 11 | 3571. | 47 | 3571. |
| 12 | 3636. | 48 | 3636. |
| 13 | 3704. | 49 | 3704. |
| 14 | 3774. | 50 | 3774. |
| 15 | 3846. | 51 | 3846. |
| 16 | 4000. | 52 | 4000. |
| 17 | 4167. | 53 | 4167. |
| 18 | 4348. | 54 | 4348. |
| 19 | 4545. | 55 | 4545. |
| 20 | 4762. | 56 | 4762. |
| 21 | 5000. | 57 | 5000. |
| 22 | 6452. | 58 | 6452. |
| 23 | 9434. | 59 | 9434. |
| 24 | 11905. | 60 | 11905. |
| 25 | 12500. | 61 | 12500. |
| 26 | 13149. | 62 | 13149. |
| 27 | 13333. | 63 | 13333. |
| 28 | 14286. | 64 | 14286. |
| 29 | 16667. | 65 | 16667. |
| 30 | 18182. | 66 | 18182. |
| 31 | 20000. | 67 | 20000. |
| 32 | 25000. | 68 | 25000. |
| 33 | 32258. | 69 | 32258. |
| 34 | 39216. | 70 | 39216. |
| 35 | 63091. | | |

## DNA DISTRIBUTION LIST

Defense Documentation Center

Defense Advanced Research Project Agency
- J. Jenny
- J. Larson
- C. Thomas
- S. Zakanycz

Defense Nuclear Agency
- R. Bigoni
- C. Blank
- H. Fitz, Jr.
- P. Hass
- J. Mayo
- G. Soper
- FCPR Field Command
- TISI Archives
- Technical Library

Defense Research and Engineering
- D. Brockway
- R. Ruffine

U.S. Air Force

Air Staff
- E. Cohen
- H. Stears

Air Force Systems Command
- D. Beadner
- W. Castlen
- R. Dietz
- W. Gallie

Air Force Geophysics Laboratory
- J.S. Garing
- R. Narcisi
- A.T. Stair, Jr.
- W. Swider
- J. Ulwick

Air Force Technical Applications Center
- J. Lange
- M. Snyder
- P. Towles
- R. Zwirmbaum

Air Force Weapons Laboratory
    G. Ganong

Space and Missile Systems Organization
    R. Baumgartner
    L. Doan
    R. Hayden
    J. Higgins
    R. Lawhern
    J. Lyons
    J. McCormac
    R. Willhite

U.S. Army

Atmospheric Sciences Laboratory
    F. Niles
    R. Olsen
    D. Snyder

BMD Advanced Technology Center
    W. Davies

U.S. Navy

Naval Research Laboratory
    T. Coffee
    D. Strobel
    Technical Library

Contractors

Aerodyne Research Inc.
    F. Bien
    M. Camac
    J. Draper

Brown Engineering Company, Inc.
    W. Barnes

University of Denver
    D. Murcray

General Electric Co. -Tempo Div.
    T. Stephens

General Electric Co. - Valley Forge
    J. Burns

General Research Corp.
J. Ise

Geophysical Institute- Univ. of Alaska
N. Brown
N. Davis
T. Hallinan
G. Romick

JCI
J. Jamieson

Lockheed Missiles and Space Co.
J. Kumer
B. Sears

Institute for Defense Analysis
E. Bauer
H. Wolfhard

Mission Research Corporation
D. Archer
D. Sappenfield

Photometrics Inc.
G. Davidson
J. Kofsky
D. Villanucci

Physical Sciences Inc.
G. Caledonia
K. Wray

R&D Associates
F. Gilmore
R. Lelevier
H. Mitchell

Science Applications Inc.
D. Hamlin
E. Hyman

Space Data Corporation
E. Allen

Stanford Research Institute
M. Baron
W. Berning
W. Chestnut

Stewart Radiance Laboratory
R. Huppi
J. Kemp

Technology International Corp.
W. Boquist

Utah State University
D. Baker
K. Baker
D. Burt
G. Frodsham
A. Steed
C. Wyatt

Visidyne Inc.
J. Carpenter
T. Degges
C. Humphrey
A. Hurd
W. Reidy